Check for updates

IUBMB Life

WILEY

RESEARCH ARTICLE

4-Methylumbelliferone Sensitizes Breast Cancer Spheroids to Chemotherapeutic Treatment With Epirubicin: New Perspectives for Pharmacological Repositioning

Daiana Luján Vitale[1,2] | Antonella Icardi[1,2] | Paolo Rosales[1,2] | Candela Morán[1,2] | Ina Sevic[1,2] | Laura Daniela Alaniz[1,2]

[1]Laboratorio de Microambiente Tumoral – Centro de Investigaciones Básicas y Aplicadas (CIBA) – Universidad Nacional del Noroeste de la Provincia de Buenos Aires, Junín, Argentina | [2]Centro de Investigaciones y Transferencia del Noroeste de la Provincia de Buenos Aires (CITNOBA) – UNNOBA-UNSAdA-CONICET, Junín, Argentina

Correspondence: Daiana Luján Vitale (dlvitale@comunidad.unnoba.edu.ar)

Received: 10 June 2025 | **Revised:** 22 October 2025 | **Accepted:** 28 October 2025

Funding: This research was funded by: BID—PICT 2021 (No. 01060) to Laura Alaniz and BID—PICT 2021 (No. 00793) to Ina Sevic (Agencia Nacional de Promoción de la Investigación, el Desarrollo Tecnológico y la Innovación); Subsidio de investigación bianuales (SIB) UNNOBA (No. 5610/2024) to Laura Alaniz and Daiana Luján Vitale; HORIZON-MSCA-2021-SE-01 (ID 101086476 CARES) to Laura Daniela Alaniz.

Keywords: 4-methylumbelliferone | breast cancer | drug repositioning | epirubicin | hyaluronan

ABSTRACT

Chemoresistance remains a significant hurdle in breast cancer treatment. To address this, we explored the therapeutic potential of combining epirubicin, an anthracycline commonly associated with the development of resistance in cancer cells and with known cytotoxic effects, with 4-methylumbelliferone, a plant-derived coumarin. Our results demonstrated a coactive enhancement of epirubicin efficacy when this combination was applied to 3D breast cancer models, irrespective of molecular subtype. Mechanistically, 4-methylumbelliferone inhibits synthesis of hyaluronan, a key component of the tumor microenvironment that promotes tumor growth and metastasis. By disrupting hyaluronan production, this compound facilitated drug penetration into tumor spheroids and reduced the expression of drug efflux pumps, thereby increasing intracellular drug accumulation. Consequently, the combined treatment led to a significant reduction in cell viability and promotion of cell death. Our findings suggest that targeting hyaluronan metabolism in conjunction with conventional chemotherapy offers a promising strategy to overcome drug resistance in breast cancer. This drug repositioning approach not only improves treatment efficacy but also highlights the potential of targeting the tumor microenvironment to enhance cancer therapy. Further studies are warranted to elucidate the underlying mechanisms and to evaluate the clinical translation of this combination therapy.

1 | Introduction

Advances in cancer genomics have revealed diverse mechanisms underlying tumor progression. Despite these insights, translating preclinical findings into effective therapies remains a significant challenge, often hindered by the emergence of drug resistance. In recent decades there has been a growing interest in the role of the extracellular matrix (ECM) in modulating drug resistance within cancer [1, 2]. The tumor stroma is characterized by an altered ECM, with variations in composition, structure, and abundance that evolve throughout tumor progression and across different tumor types. Notably, many tumors exhibit an

Abbreviations: 4-MU, 4-methylumbelliferone; ECM, extracellular matrix; EPI, epirubicin; GAG, glycosaminoglycan; GlcNAc, *N*-acetyl-D-glucosamine; GlcUA, D-glucuronic acid; HA, hyaluronan; HAS, hyaluronan synthase; HYAL, hyaluronidase; TNBC, triple-negative breast cancer; UGDH, UDP-glucose dehydrogenase.

Antonella Icardi and Paolo Rosales contributed equally to this work.

© 2025 International Union of Biochemistry and Molecular Biology.

enrichment of glycosaminoglycan (GAG) hyaluronan (HA). HA is a linear polysaccharide synthesized by hyaluronan synthases (HAS) from *N*-acetyl-D-glucosamine (GlcNAc) and D-glucuronic acid (GlcUA) units, requiring UDP conjugation for recognition by HASs. Conversely, hyaluronidases (HYAL) are endoglycosidases responsible for HA degradation. Dysregulation of these enzymes has been implicated in various pathologies, including cancer [3, 4].

A promising avenue for addressing the challenges of drug resistance is drug repositioning, which involves repurposing existing, well-characterized medications for new disease indications. This strategy offers a significant advantage by reducing the time and costs typically associated with developing novel oncological treatments. Moreover, drug repositioning can uncover novel mechanisms of action and facilitate the creation of more effective therapeutic combinations, expanding the range of treatment options available for cancer patients [5–7].

Anthracyclines, such as epirubicin (EPI), are widely used chemotherapy drugs for breast cancer treatment [8]. Despite advances in targeted therapies, EPI remains a valuable option, especially for triple-negative breast cancer (TNBC), due to its effectiveness and affordability. TNBC, characterized by its aggressive nature and resistance to hormonal therapy, often poses significant treatment challenges. While luminal breast cancer typically responds to hormonal therapy, EPI may be used in cases of resistance [9]. The development of resistance to EPI associated with mechanisms involved in its metabolization and elimination from tumor cells have been reported [10–12]. Glucuronidation, catalyzed by UDP-glucuronosyltransferase 7 (UGT2B7), is the primary inactivation pathway for EPI. This enzyme conjugates EPI to glucuronic acid (GlcUA), which requires UDP conjugation for recognition. Interestingly, UDP-GlcUA serves a dual function: it acts as both a glucuronidation substrate and a precursor for the synthesis of HA and other ECM proteoglycans. UDP-glucose dehydrogenase (UGDH), the enzyme responsible for UDP-GlcUA formation [13], acts as a metabolic checkpoint, influencing both glycosylation pathways and ECM synthesis, while also impacting drug inactivation by glucuronidation.

4-methylumbelliferone (4-MU), a coumarin derivative approved for liver conditions in Europe and Asia, has been shown to inhibit HA production. 4-MU acts as a competitive substrate for UDP, reducing the cell availability of GlcUA, a precursor for both HA synthesis and EPI glucuronidation [14]. Additionally, 4-MU downregulates the expression of enzymes involved in HA synthesis and UDP-GlcUA production [15]. This dual action on HA synthesis and EPI metabolism suggests that combining 4-MU with EPI could potentially enhance the efficacy of EPI treatment while potentially mitigating its toxicity. While 4-MU has been studied in various cancers [16], the lack of scientific evidence supporting its approval for this purpose poses a significant challenge. However, the potential benefits of combining 4-MU with EPI in breast cancer treatment warrant further exploration. Given the effects of 4-MU on EPI glucuronidation and HA synthesis, we hypothesized that combining 4-MU with EPI could enhance the antitumor activity of EPI while modifying the pro-tumorigenic effects of an altered ECM. By reducing EPI glucuronidation, 4-MU could potentially increase EPI's intracellular concentration and activity, leading to enhanced tumor cell death. Simultaneously, by inhibiting HA and other GAG synthesis, 4-MU could potentially disrupt the tumor microenvironment and reduce tumor progression. To investigate this hypothesis, we conducted studies combining EPI and 4-MU treatments in two breast cancer models.

2 | Results

2.1 | Effect of EPI and 4-MU Treatment on the Cellular Integrity of Tumor Spheroids

To assess the effects of EPI and 4-MU on cell integrity and survival, the viability of MDA-MB-231 and MCF-7 spheroids was determined after 3 days of each treatment using an MTS assay (Figure 1A). First, when comparing the OD values of both untreated spheroid types (BC), we observed a higher basal viability in MCF-7 compared to MDA-MB-231 spheroids. This may be related to the organization of the spheroids and the expression of adhesion markers, which are necessary for spheroid compaction and formation, and are related with its viability.

As expected, MDA-MB-231 spheroids treated with 2.5 μM EPI (EPI) showed approximately a 10% reduction in viability compared to untreated spheroids (BC) ($p < 0.05$). Notably, treatment with 0.5 mM 4-MU alone did not significantly alter cell viability compared to BC. Interestingly, EPI + 4-MU treatment reduced cell viability by 20% compared to BC ($p < 0.01$), demonstrating a higher effect than that produced by 4-MU alone ($p < 0.05$) (Figure 1A). Similar evaluations were performed on MCF-7 spheroids (Figure 1D), where the combination of 1.5 μM EPI and 0.5 mM 4-MU induced a 50% reduction in cell viability compared to BC ($p < 0.0001$). Furthermore, the effect of EPI + 4-MU treatment was more effective in reducing cell viability compared with EPI alone ($p < 0.001$). This result further shows that the presence of 4-MU during EPI treatment enhances the drug response in this tumor model as well. Unexpectedly, 4-MU treatment decreased cell viability in relation to control spheroids (approximately 30%) ($p < 0.001$) (Figure 1D), prompting us to conduct additional assays to rule out potential toxic effects of 4-MU in MCF-7 spheroids.

To further investigate the effects of EPI + 4-MU treatment on cytotoxicity, we evaluated LDH activity in spheroid supernatants. Notably, we did not observe significant differences in LDH activity between treated and not treated MDA-MB-231 (Figure 1B) or MCF-7 spheroids (Figure 1E). This finding suggests that EPI + 4-MU treatment might influence tumor cell viability without inducing the release of intracellular contents into the extracellular environment, potentially contributing to inflammatory or cytotoxic conditions. Moreover, this result allows us to rule out any toxic effects at the cellular and extracellular levels caused by 4-MU in MCF-7 spheroids. Considering these results and the antiproliferative functions of EPI as a DNA intercalator, a cytostatic effect mediated by the EPI + 4-MU combination could be proposed.

To assess early apoptosis induction, we determined the percentage of annexin-V+ cells following EPI + 4-MU treatment by flow cytometry. Due to the intrinsic characteristics of the 3D spheroid model, baseline apoptosis levels in MDA-MB-231 (Figure 1C) and MCF-7 (Figure 1F) spheroids were relatively high, finding two well-distinguished cell populations according to the distinctive organizational and 3D properties of tumor spheroids

15216551, 2025, 11, Downloaded from https://iubmb.onlinelibrary.wiley.com/doi/10.1002/iub.70075 by Daiana L. Viale - UNNOBA Uni Nacional del Noroeste de la Provincia de Buenos A. , Wiley Online Library on [10/11/2025]. See the Terms and Conditions (https://onlinelibrary.wiley.com/terms-and-conditions) on Wiley Online Library for rules of use; OA articles are governed by the applicable Creative Commons License

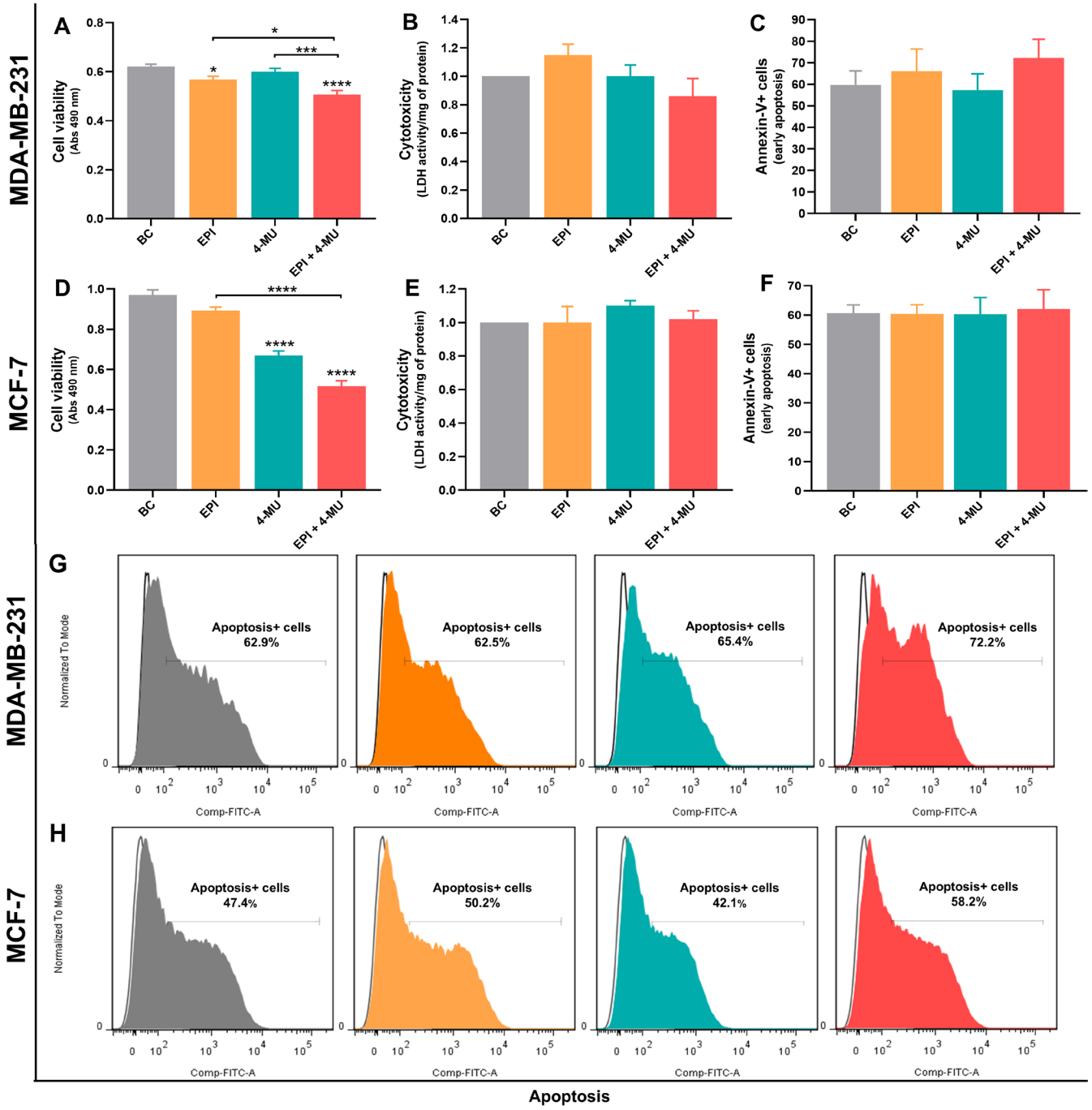


FIGURE 1 | Effect of treatment with EPI in the presence of 4-MU on the integrity of tumor cells. MDA-MB-231 or MCF-7 cells (8×10^3) were cultured under three-dimensional conditions using the hanging drop assay to allow the formation of tumor spheroids. On day 5, the spheroids were treated with 0.5 mM 4-MU plus 1.5 μM EPI (MCF-7) or 0.5 mM 4-MU plus 2.5 μM EPI (MDA-MB-231) for 3 days. On day 8, different spheroids per condition were collected and cell viability was determined by MTS (A, $N=6$ and D, $N=7$) and early apoptosis by flow cytometry (C, F, G, H, $N=3$). To determine cytotoxicity, supernatants from different spheroids were collected and LDH activity was determined (B and E, $N=3$). Histograms (G and H) show the most representative data from three independent experiments performed with at least 50,000 events/condition. Mean ± SEM. $^*p<0.05$, $^{**}p<0.01$, $^{***}p<0.001$, $^{****}p<0.0001$.

(Figure 1G,H). High apoptosis rates could limit the ability to distinguish possible differences between the proposed treatments. Thus, when analyzing the overall percentage of apoptotic cells, we did not observe significant differences in early apoptosis induction between treated and untreated spheroids derived from either of the two cell lines.

2.2 | Effect of 4-MU on EPI Accumulation in BC Cells

Subsequently, we evaluated the impact of adding 4-MU to chemotherapeutic treatment with EPI. In general, we found that 4-MU significantly potentiated the intracellular accumulation

15216551, 2025, 11, Downloaded from https://iubmb.onlinelibrary.wiley.com/doi/10.1002/iub.70075 by Daiana L. Viale - UNNOBA Uni Nacional del Noroeste de la Provincia de Buenos A , Wiley Online Library on [10/11/2025]. See the Terms and Conditions (https://onlinelibrary.wiley.com/terms-and-conditions) on Wiley Online Library for rules of use; OA articles are governed by the applicable Creative Commons License

of EPI in both tumor models. Notably, we observed a significant increase of approximately 50% in the amount of EPI+ MDA-MB-231 cells in the presence of 4-MU (EPI + 4-MU) compared to cells treated only with EPI (EPI) ($p < 0.05$) (Figure 2A). In line with the percentage of EPI+ cells, the intracellular accumulation of EPI per cell (MFI) significantly increased in MDA-MB-231 spheroids treated with EPI + 4-MU compared to spheroids treated with EPI alone ($p < 0.05$) (Figure 2B). In other words, these tumor cells accumulated a greater amount of EPI in the presence of 4-MU, as indicated by MFI.

The same analysis was conducted using cells derived from MCF-7 spheroids treated with EPI or EPI + 4-MU. In this case, we also observed an increase of about 13% in the number of EPI+ cells when spheroids were treated with EPI + 4-MU compared to cells from spheroids treated only with EPI ($p < 0.05$) (Figure 2C). However, when we analyzed the intracellular accumulation of EPI per cell (MFI), no differences were observed (Figure 2D). When evaluating cell populations characteristics, we also observed differences related to the tumor cell type. In cells derived from MDA-MB-231 spheroids, we observed a homogeneous population with respect to EPI accumulation, which changed its MFI during treatment with EPI + 4-MU (Figure 2E). Conversely, in cells derived from MCF-7 spheroids, we observed two well-differentiated populations in terms of EPI accumulation capacity: one negative and the other positive (Figure 2F).

Given that the total percentage of apoptotic cells did not reflect differences in cell death induction between treatments, and considering the 3D characteristics of the spheroids, we characterized different cell populations taking into account both apoptosis induction and EPI accumulation. Annexin-V was employed as a marker of early apoptosis, and cell populations were analyzed considering intracellular EPI accumulation as well. We observed a higher percentage of EPI+ and apoptotic cells (annexin-V+ cells) in the presence of 4-MU in both tumor spheroid models (Figure 2G). This indicates a population of apoptotic cells that had incorporated the drug into spheroids treated with the EPI + 4-MU combination compared to EPI alone. This observation prompted a deeper investigation into the potential differential impact of 4-MU on apoptosis in tumor cells that had incorporated EPI, reflecting their sensitivity to the antitumor treatment.

Consequently, we focused on the tumor cell population exhibiting both apoptosis and EPI (EPI^+/$apoptosis^+$ population). Considering the 3D organization of spheroids, cells meeting these characteristics could be classified as sensitive to EPI. These cells could correspond to those that incorporated the drug and underwent cell death. Therefore, we compared the MFI for both markers as a measure of the amount of drug accumulated and the induction of apoptosis under proposed treatments. In cells derived from MDA-MB-231 spheroids, we detected elevated cell death and increased intracellular EPI accumulation per cell in the EPI + 4-MU group compared to the EPI-only group determined by the MFI values ($p < 0.05$) (Figure 2H). On the other hand, evaluating the EPI+/apoptosis+ population derived from MCF-7 spheroids revealed no significant differences in apoptosis induction as measured by annexin-V MFI (Figure 2I). These results corroborate the notion that 4-MU enhances both EPI accumulation within spheroids and the apoptosis rate of tumor cells that exhibited higher intracellular EPI accumulation. This suggests that tumor cells not only effectively incorporate and retain EPI but also become more sensitive to its apoptosis-inducing effects, as manifested by the increase in cell death. This phenomenon was particularly pronounced in the MDA-MB-231 model, again highlighting the differences between the two tumor models.

Given that the total percentage of early apoptotic cells measured by Annexin V staining did not reveal significant differences in cell death induction between treatments, and considering caspase-3 cleavage and activation as a late marker of apoptosis, we evaluated cytoplasmic levels of cleaved caspase-3 (CC3) by intracellular flow cytometry in MDA-MB-231 spheroids (Figure S1). Two distinct cell populations—CC3-positive (CC3+) and CC3-negative (CC3−)—were observed, consistent with the intrinsic heterogeneity of the spheroid model. However, no significant differences were found in the percentage of CC3+ cells or in MFI across treatments. Notably, MCF-7 spheroids were not analyzed due to their lack of caspase-3 expression.

2.3 | Effect of EPI and 4-MU Treatment on the Expression of Drug Resistance Markers

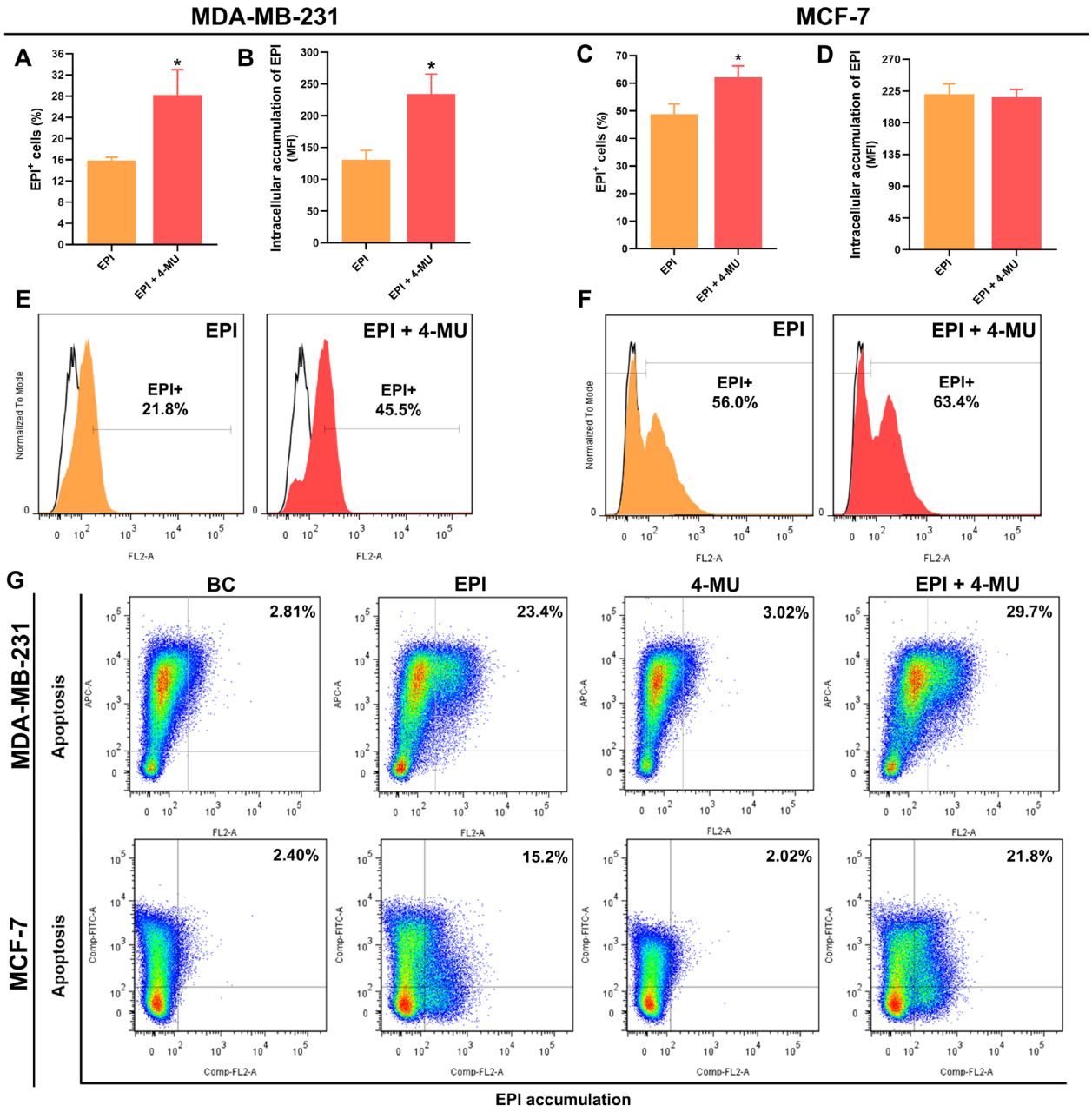
A crucial aspect of studying drug efficacy is the evaluation of resistance and progression markers, which reflect tumor cell responsiveness to chemotherapy. In this context, we examined the expression of three ATP-dependent membrane efflux pumps implicated in EPI elimination and associated with drug resistance. We analyzed ABCG2, ABCC1, and ABCC2 expression in MDA-MB-231 and MCF-7 spheroids treated with EPI + 4-MU, where we found results consistent with the previously observed enhanced EPI sensitivity.

First, we observed a significant downregulation of ABCG2 ($p < 0.001$) (Figure 3A) and ABCC2 ($p < 0.05$) (Figure 3C) in MDA-MB-231 spheroids exposed to EPI + 4-MU compared to BC. Moreover, ABCG2 expression was notably reduced when comparing EPI + 4-MU to EPI alone treatments ($p < 0.01$) (Figure 3A). Similar results were found when determining the expression of both drug efflux pumps in MCF-7 spheroids, where EPI + 4-MU treatment diminished ABCG2 and ABCC2 mRNA levels compared to basal conditions ($p < 0.001$) (Figure 3D,F). On the other hand, ABCC1 expression did not exhibit significant modulation in its synthesis (Figure 3B,E). These findings, combined with elevated EPI accumulation and enhanced apoptosis within the drug-treated population, indicate an increased sensitivity to EPI therapy in the presence of 4-MU. This effect can be attributed to both functions of 4-MU: as an inhibitor of HA synthesis, thereby altering the tumor ECM, and as a competitor for GlcUA, which enhances the efficacy of EPI.

2.4 | Effect of 4-MU and EPI Treatment on Spheroids Size

Another focus of this study was to assess potential alterations in the size and compactness of spheroids exposed to EPI and 4-MU. To this end, first we captured micrographs of multiple spheroids from each treatment group at the experimental

15216551, 2025, 11, Downloaded from https://iubmb.onlinelibrary.wiley.com/doi/10.1002/iub.70075 by Daiana L. Viale - UNNOBA Uni Nacional del Noroeste de la Provincia de Buenos A , Wiley Online Library on [10/11/2025]. See the Terms and Conditions (https://onlinelibrary.wiley.com/terms-and-conditions) on Wiley Online Library for rules of use; OA articles are governed by the applicable Creative Commons License



H

Analysis of EPI accumulation and apoptosis in MDA-MB-231 spheroids Mean Fluorescence Intensity (MFI)				
EPI⁺ / apoptosis⁺ population	**BC**	**EPI**	**4-MU**	**EPI + 4-MU**
MFI apoptosis (Mean ± SEM)	876.0 ± 49.2	1006 ± 136.3	865.5 ± 87.2	1317 ± 290.2
MFI EPI (Mean ± SEM)		137.2 ± 8.0		169.6 ± 9.9*

I

Analysis of EPI accumulation and apoptosis in MCF-7 spheroids Mean Fluorescence Intensity (MFI)				
EPI⁺ / apoptosis⁺ population	**BC**	**EPI**	**4-MU**	**EPI + 4-MU**
MFI apoptosis (Mean ± SEM)	515.3 ± 85.4	544.3 ± 78.8	538.7 ± 73.2	661.7 ± 38.5
MFI EPI (Mean ± SEM)		91.7 ± 8.6		128.6 ± 13.1

FIGURE 2 | Legend on next page.

15216551, 2025, 11, Downloaded from https://iubmb.onlinelibrary.wiley.com/doi/10.1002/iub.70075 by Daiana L. Vitale - UNNOBA Uni Nacional del Noroeste de la Provincia de Buenos A , Wiley Online Library on [10/11/2025]. See the Terms and Conditions (https://onlinelibrary.wiley.com/terms-and-conditions) on Wiley Online Library for rules of use; OA articles are governed by the applicable Creative Commons License

FIGURE 2 | Effect of 4-MU on EPI treatment and antitumoral response. MDA-MB-231 or MCF-7 cells (8×10^3) were cultured under three-dimensional conditions using the hanging drop assay to allow the formation of tumor spheroids. On day 5, the spheroids were treated with 0.5 mM 4-MU plus 1.5 μM EPI (MCF-7) or 0.5 mM 4-MU plus 2.5 μM EPI (MDA-MB-231) for 3 days. On day 8, different spheroids per condition were collected and EPI intracellular accumulation and early apoptosis were determined by flow cytometry. Intracellular EPI accumulation was measured using the FL2 detector. Early apoptosis was determined using annexin-V-FITC. Bars show the percentage of EPI+ cells (A, C, $N = 7$) or the mean fluorescence intensity (MFI) (B, D, $N = 4$) determined by comparison with a negative control. MFI of apoptosis (top) and epirubicin (EPI) (bottom) in the EPI^+/$apoptosis^+$ cell population determined by FACS analysis of MDA-MB-231 (H) and MCF-7 (I) spheroids ($N = 3$). Histograms (E, F) and dotplots (G) show the most representative experiment performed with at least 50,000 events/condition. Mean ± SEM. *$p < 0.05$.

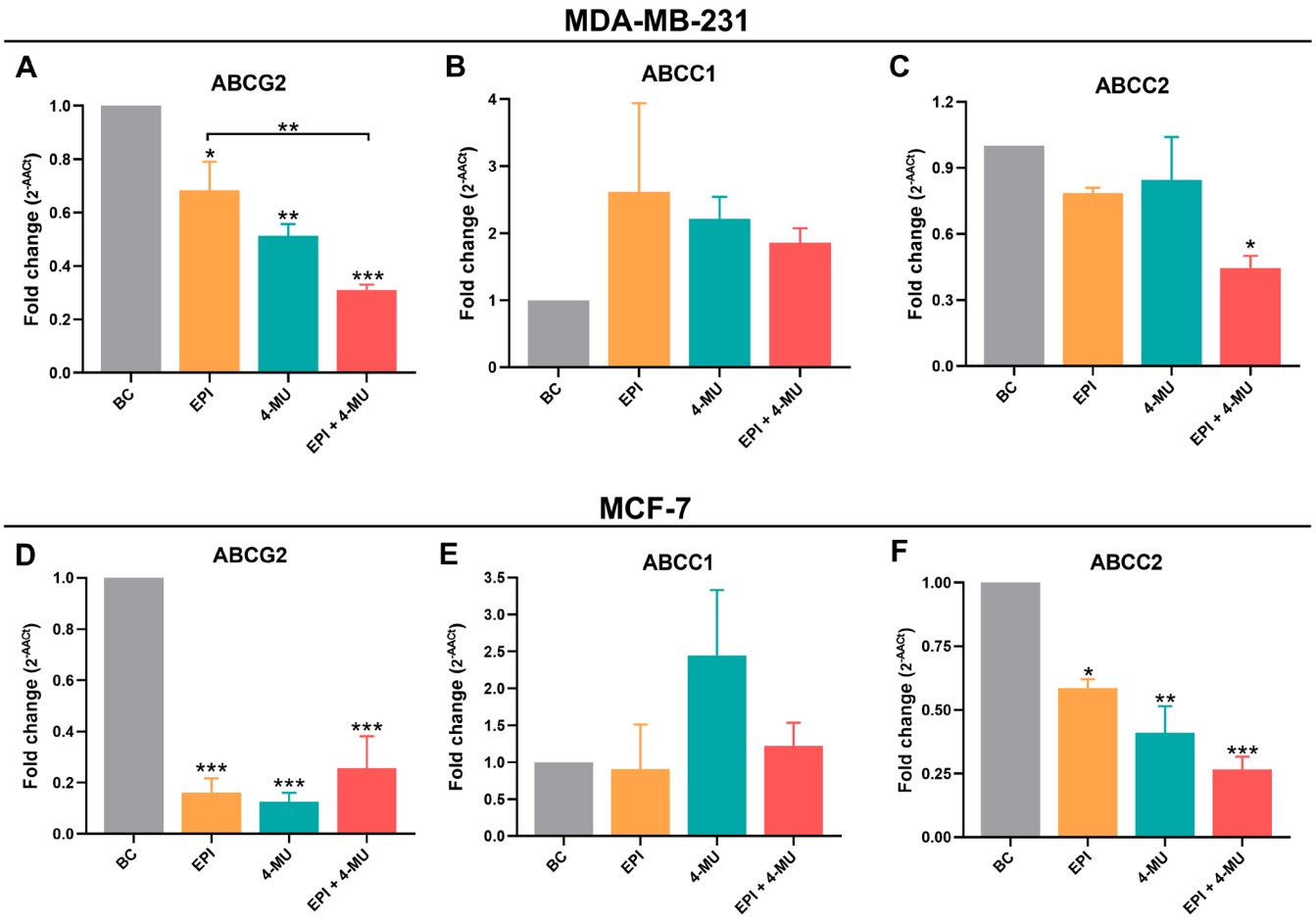


FIGURE 3 | Effect of 4-MU and EPI treatment on the expression of drug resistance markers. MDA-MB-231 or MCF-7 cells (8×10^3) were cultured under three-dimensional conditions using the hanging drop assay to allow the formation of tumor spheroids. On day 5, the spheroids were treated with 0.5 mM 4-MU plus 1.5 μM EPI (MCF-7) or 0.5 mM 4-MU plus 2.5 μM EPI (MDA-MB-231) for 3 days. On day 8, different spheroids per condition were collected. To evaluate the expression of ABCG2 (A, D), ABCC1 (B, E), and ABCC2 (C, F), total RNA was extracted, and 2 μg were reverse transcribed by RT-PCR. cDNAs were subjected to real time quantitative PCR using SYBR Green. Results were normalized using B2M as reference gene and all determinations were performed as duplicates. $N = 3$, expressed as mean ± SEM. *$p < 0.05$, **$p < 0.01$, ***$p < 0.001$.

endpoint (day 8) and computed the volume and perimeter for each condition. Spheroids generated from MDA-MB-231 cells exhibited a significant reduction in volume after 3 days of treatment with EPI, 4-MU, or EPI + 4-MU compared to untreated controls ($p < 0.001$). However, no significant differences in volume were observed among the treatment groups (Figure 4A,E). Similarly, all treatments led to a decrease in spheroid perimeter relative to controls ($p < 0.001$). Interestingly, spheroids treated with EPI + 4-MU displayed a smaller perimeter than those exposed to 4-MU ($p < 0.05$) (Figure 4B,E). A similar analysis was conducted on MCF-7 spheroids, revealing a consistent reduction in both spheroid volume and perimeter (Figure 4C–F) following all treatments compared to untreated controls. However, no significant differences in size were observed among the treatment groups.

Considering these findings and the therapeutic objective of tumor mass reduction, individually selected spheroids from each experimental condition were identified to determine their areas prior to treatment (day 5) and posttreatment (day 8). This enabled us to examine the temporal dynamics of potential size alterations, treating each spheroid as a unique entity

15216551, 2025, 11, Downloaded from https://iubmb.onlinelibrary.wiley.com/doi/10.1002/iub.70075 by Daiana L. Vitale - UNNOBA Uni Nacional del Noroeste de la Provincia de Buenos A , Wiley Online Library on [10/11/2025]. See the Terms and Conditions (https://onlinelibrary.wiley.com/terms-and-conditions) on Wiley Online Library for rules of use; OA articles are governed by the applicable Creative Commons License

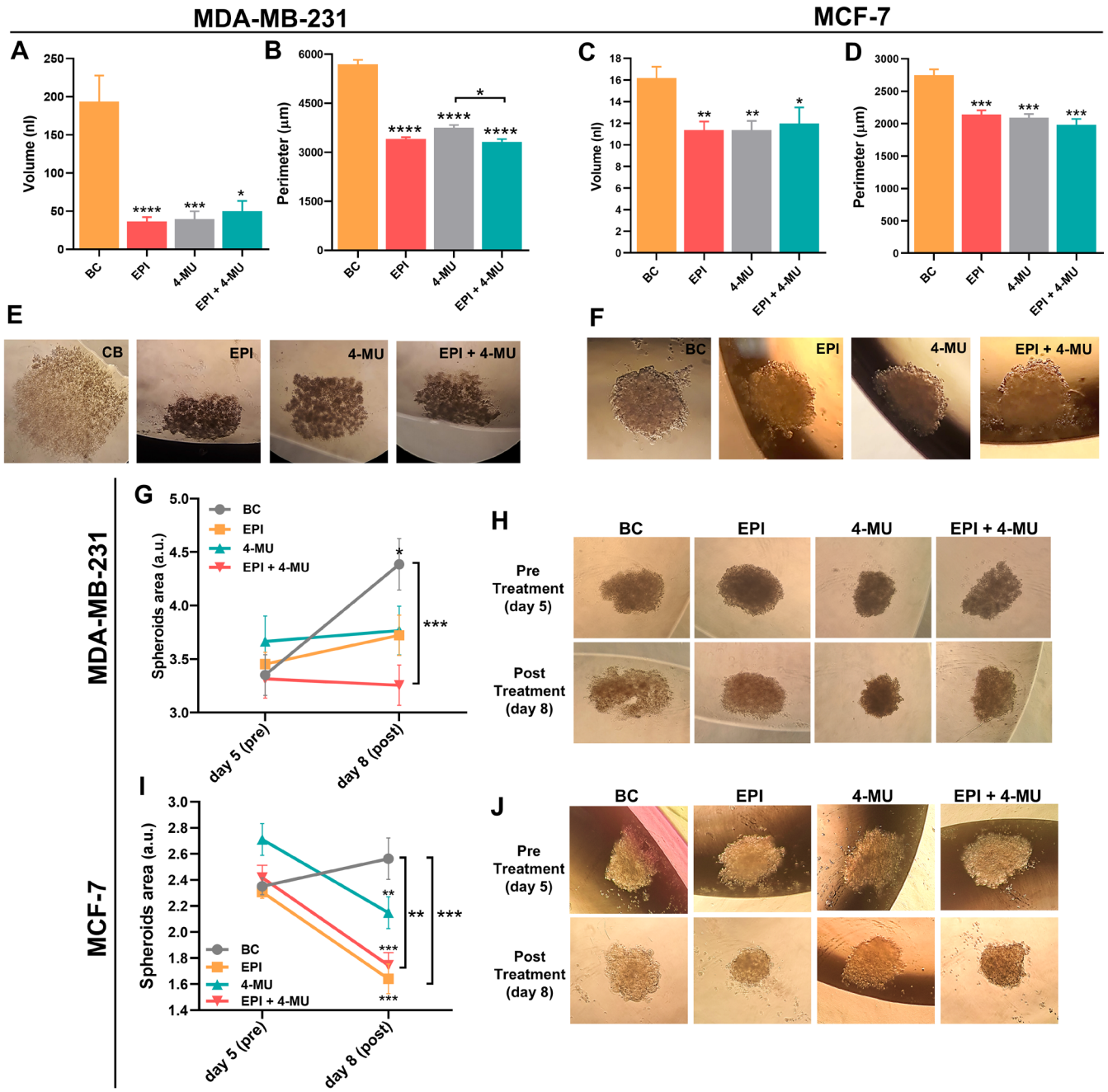


FIGURE 4 | Effect of 4-MU and EPI treatment on spheroid size and compaction. MDA-MB-231 or MCF-7 cells (8×10^3) were cultured under three-dimensional conditions using the hanging drop assay to allow the formation of tumor spheroids. On day 5, the spheroids were treated with 0.5 mM 4-MU plus 1.5 µM EPI (MCF-7) or 0.5 mM 4-MU plus 2.5 µM EPI (MDA-MB-231) for 3 days. On day 8, different spheroids per condition were collected and several micrographs were taken to calculate spheroid volume (A, C) and perimeter (B, D). For the calculation of spheroid size, on day 5 (pretreatment) and day 8 (posttreatment), different micrographs of each spheroid were taken and analyzed with ImageJ software (E, F, H, J). Expressed as mean ± SEM. *$p < 0.05$, **$p < 0.01$, ***$p < 0.001$.

(Figure 4G–J). Evaluation of MDA-MB-231 spheroid area at day 5 (pretreatment) and day 8 (posttreatment) revealed an expected increase in size for the untreated control group ($p < 0.05$), mimicking in vivo tumor growth (Figure 4G,H). Spheroids treated with EPI, 4-MU, or the combination showed no significant size differences compared to BC. Nevertheless, when an exhaustive analysis of two variables (time and treatments) was performed, the only treatment condition that reduced spheroid size compared to BC was EPI + 4-MU ($p < 0.001$) (Figure 4G,H).

The same methodological approach was applied to MCF-7 spheroids, which demonstrated distinct behavior compared to MDA-MB-231. Firstly, no differences were observed in the size of the untreated spheroids between day 5 and day 8 of culture (Figure 4I,J). This finding might correlate with a diminished rate of tumor growth and progression in this model when compared to MDA-MB-231. Furthermore, a reduction in MCF-7 spheroids size was observed when comparing day 5 to day 8 of culture within each treatment, including EPI (4-MU, $p < 0.01$; EPI, $p < 0.001$; EPI + 4-MU, $p < 0.001$). This demonstrates an

15216551, 2025, 11, Downloaded from https://iubmb.onlinelibrary.wiley.com/doi/10.1002/iub.70075 by Daiana L. Viale - UNNOBA Uni Nacional del Noroeste de la Provincia de Buenos A , Wiley Online Library on [10/11/2025]. See the Terms and Conditions (https://onlinelibrary.wiley.com/terms-and-conditions) on Wiley Online Library for rules of use; OA articles are governed by the applicable Creative Commons License

intrinsic sensitivity to EPI, which we had not observed in the MDA-MB-231 model. Moreover, the reduction in tumor size observed with the EPI + 4-MU treatment is also attributable to the effect of EPI itself (Figure 4I,J). These results, for both cell lines, indicate that treatment with EPI in the presence of 4-MU not only increases the accumulation of the chemotherapeutic drug but also enhances cell death by apoptosis and reduces spheroid size compared to untreated spheroids. Moreover, results suggest that the reduction in spheroid size could be also related to a potential cytostatic effect of EPI+ 4-MU treatment, that affects the proliferative capacity of the cells. Finally, a comparison between the responses of both breast cancer models is possible, as MCF-7 spheroids exhibited greater sensitivity to EPI as a chemotherapeutic agent.

2.5 | Effect of 4-MU and EPI Treatment on HA Synthesis and Accumulation in ECM

We further aimed to investigate the modulation of HA biosynthesis by EPI and 4-MU treatment and its accumulation within the ECM of tumor spheroids. To this end, we initiated our analysis by assessing HA levels using flow cytometry. Initially, we quantified HA pericellular production in MDA-MB-231 cells derived from spheroids by flow cytometry. First, we observed results similar to those previously reported regarding a high expression and accumulation of HA in MDA-MB-231 cells (Figure 5A–C). When evaluating HA production per cell, as measured by MFI, the only treatment significantly decreasing HA production was 4-MU (Figure 5A). These findings confirm that 4-MU reduces HA synthesis in this 3D model. Upon analyzing the percentage of HA+ cells, we found that a substantial proportion of cells originated from spheroids exhibited HA within their ECM together with only a small percentage of HA− cells (Figure 5C). This could be due to the high number of HA+ cells, which may have made it difficult to obtain noticeable differences between the proposed treatments.

Given the 3D architecture of spheroids, we characterized different cell populations within MDA-MB-231 spheroids based on EPI accumulation and HA synthesis, as both processes are significantly influenced by 4-MU treatment (Figure S5). In spheroids treated with EPI + 4-MU a significant reduction in the EPI-/HA+ population (light blue) was observed in the presence of 4-MU compared to untreated conditions ($p < 0.01$) (Figure S5). This could indicate that the number of cells expressing HA in their ECM, but not containing EPI inside, was reduced. On the other hand, the EPI+/HA+ population (orange) increased compared to EPI treatment alone ($p < 0.05$). These findings suggest that the effect of 4-MU on HA synthesis was more pronounced in the absence of EPI. These results are consistent with the fact that, in cells that incorporated EPI, the effect of 4-MU on GlcUA arrest could be divided between the two processes mediated by it: the inactivation of EPI and the synthesis of HA and other GAGs not analyzed in the present work.

We continued investigating the amount of HA present in spheroids from the different treatments, observing a significant decrease in HA fluorescence intensity after 4-MU treatment compared to BC ($p < 0.05$) (Figure 5E,F), as previously shown by flow cytometry (Figure 5A). Furthermore, this effect of 4-MU on HA synthesis was also observed when spheroids were treated in combination with EPI (EPI + 4-MU) ($p < 0.05$) (Figure 5D,E). Importantly, we ruled out that the observed reduction in HA synthesis was not affected by a reduction in spheroid size since correlation analyzes demonstrated that there is no association between the amount of HA in each spheroid and its area (Figure 5G), or perimeter (Figure 5H). On the other hand, by analyzing DAPI fluorescence intensity in untreated spheroids, we observed the maintenance of the characteristic three-dimensional organization. Specifically, we observed a more proliferative area located at the periphery, related to a high fluorescence intensity, and a center with lower intensity, which could be associated with a necrotic or apoptotic region (Figure 5D). When quantifying this parameter and comparing it among the different experimental groups, both EPI treatment and the combined treatment with EPI + 4-MU achieved a marked decrease in DAPI fluorescence intensity compared to untreated spheroids ($p < 0.0001$) (Figure 5F). Furthermore, correlation analyzes between DAPI fluorescence intensity and spheroid area (Figure 5I) and perimeter (Figure 5J) revealed a significant positive association. This indicates that a decrease in DAPI fluorescence intensity is associated with a decrease in spheroid size. Therefore, evaluating DAPI intensity as an individual parameter also supported the previously observed reduction in spheroid size and increased cell death by apoptosis.

We employed the same methodological approach using MCF-7 spheroids (Figure 6). First, we evaluated HA synthesis per cell, determined by mean fluorescence intensity (MFI) (Figure 6A), and the percentage of HA+ cells in this tumor model (Figure 6B,C). In general, cells derived from MCF-7 spheroids exhibited lower HA synthesis and a lower percentage of HA+ cells compared to MDA-MB-231 cells. However, no significant differences were observed in either parameter when comparing treated MCF-7 spheroids to controls. We then conducted a parallel analysis of HA pericellular accumulation and EPI accumulation, where no statistically significant differences were also observed (Figure S2).

Subsequently, we performed fluorescence microscopy to determine HA synthesis and accumulation, along with DAPI as a nuclear marker (Figure 6D). As expected, we observed a marked decrease in HA production in spheroids treated with 4-MU compared to BC ($p < 0.01$). Furthermore, during EPI + 4-MU treatment, 4-MU significantly diminishes HA synthesis ($p < 0.05$). This result was also supported by a decrease in HA fluorescence intensity between the EPI alone treatment and the combined EPI + 4-MU treatment ($p < 0.0001$) (Figure 6E). We again ruled out that the lower fluorescence intensity was due to a reduction in spheroid size by correlating it with the area (Figure 6G) and perimeter (Figure 6H) of the analyzed spheroids. These results were consistent with those observed in MDA-MB-231 spheroids. On the other hand, quantifying the fluorescence intensity for DAPI yielded unexpected results, with increased fluorescence intensity in spheroids treated with 4-MU ($p < 0.0001$) and EPI + 4-MU ($p < 0.01$) compared to BC (Figure 6F). However, we believe these results do not affect the findings for HA since

15216551, 2025, 11, Downloaded from https://iubmb.onlinelibrary.wiley.com/doi/10.1002/iub.70075 by Daiana L. Viale - UNNOBA Uni Nacional del Noroeste de la Provincia de Buenos A. , Wiley Online Library on [10/11/2025]. See the Terms and Conditions (https://onlinelibrary.wiley.com/terms-and-conditions) on Wiley Online Library for rules of use; OA articles are governed by the applicable Creative Commons License

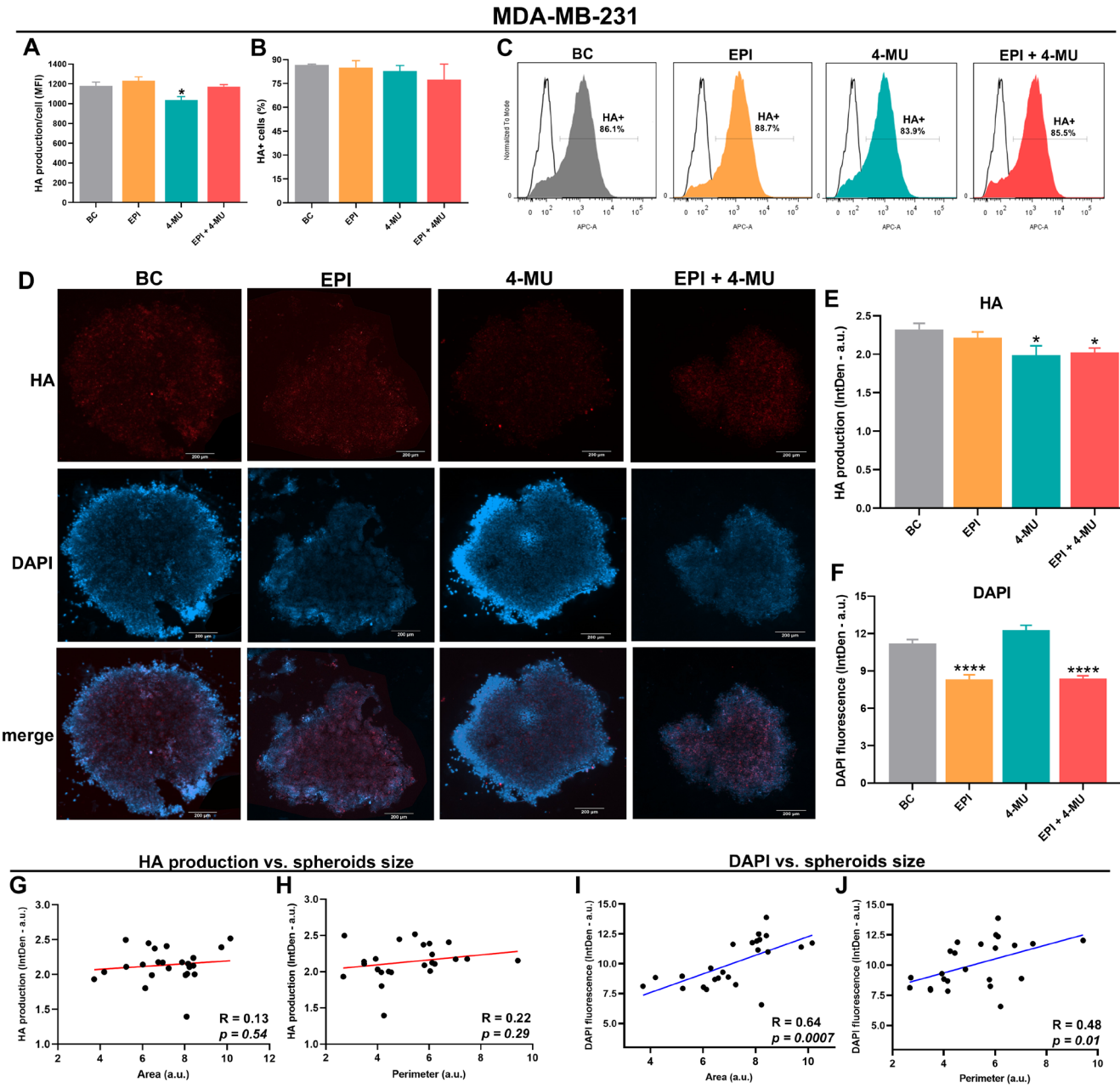


FIGURE 5 | Effect of 4-MU and EPI treatment on HA synthesis and accumulation in MDA-MB-231 spheroids. MDA-MB-231 cells (8×10^3) were cultured under three-dimensional conditions using the hanging drop assay to allow the formation of tumor spheroids. On day 5, the spheroids were treated with 0.5 mM 4-MU plus 2.5 μM EPI for 3 days. After the spheroids were treated (day 8), different spheroids per condition were collected and HA synthesis and pericelular accumulation were determined by flow cytometry (A–C). HA production and accumulation (D red, E) in tumor spheroids were determined by fluorescent microscopy. Nuclei of MDA-MB-231 cells were detected with DAPI (D blue, F). HA production and DAPI staining were compared to spheroids size by correlation analyzes (G–J). Histograms, dotplots and images show the most representative data. Scale bar: 200 μm. Mean ± SEM. *$p < 0.05$, **$p < 0.01$, ***$p < 0.001$, ****$p < 0.0001$.

there was no correlation between changes in spheroid size and DAPI fluorescence intensity (Figure 6I,J).

2.6 | Effect of 4-MU and EPI Treatment on the Expression of HA-Related Genes

Given the critical involvement of HA accumulation in the tumor microenvironment, we aimed to investigate the potential modulatory effects of 4-MU on expression profiles of key enzymes implicated in HA metabolism. Initially, a substantial reduction in HAS-2 expression was observed across all treatment groups (EPI, 4-MU and EPI + 4-MU) compared to control spheroids within the MDA-MB-231 cell line ($p < 0.001$, $p < 0.01$, $p < 0.0001$ respectively) (Figure 7A). While also a decrease in HAS-2 expression was evident in MCF-7 spheroids, statistical analysis did not reveal significant differences (Figure 7G). Furthermore, UGDH expression, a critical enzyme in UDP-GlcUA biosynthesis, exhibited a nearly 50% decrease in MDA-MB-231 spheroids treated with the EPI + 4-MU compared to the untreated spheroids ($p < 0.05$) (Figure 7B). A similar reduction in UGDH expression was

15216551, 2025, 11, Downloaded from https://iubmb.onlinelibrary.wiley.com/doi/10.1002/iub.70075 by Daiana L. Vitale - UNNOBA Uni Nacional del Noroeste de la Provincia de Buenos A. , Wiley Online Library on [10/11/2025]. See the Terms and Conditions (https://onlinelibrary.wiley.com/terms-and-conditions) on Wiley Online Library for rules of use; OA articles are governed by the applicable Creative Commons License

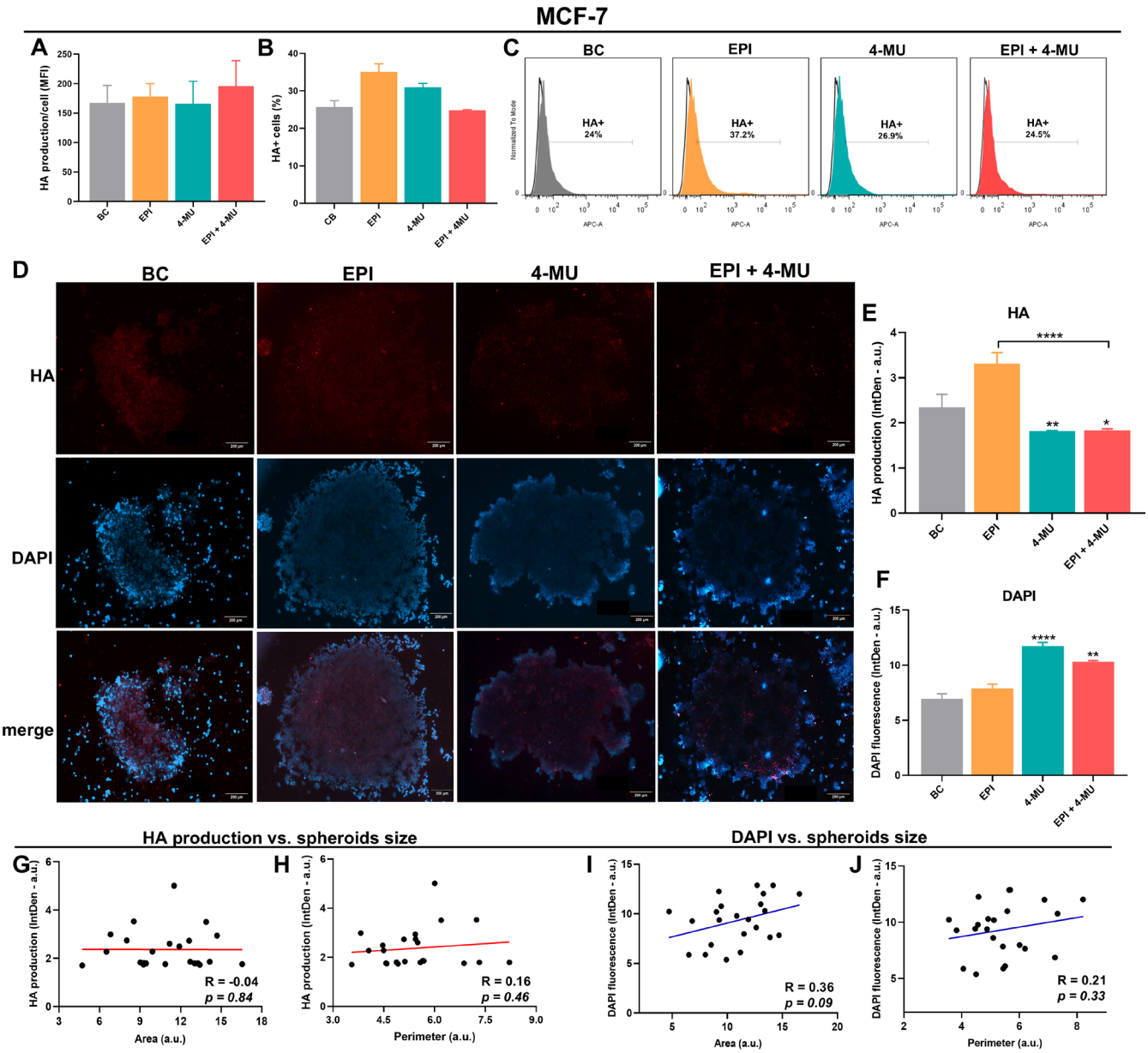


FIGURE 6 | Effect of 4-MU and EPI treatment on HA synthesis and accumulation in MCF-7 spheroids. MCF-7 cells (8×10^3) were cultured under three-dimensional conditions using the hanging drop assay to allow the formation of tumor spheroids. On day 5, the spheroids were treated with 0.5 mM 4-MU plus 1.5 μM EPI for 3 days. After the spheroids were treated (day 8), different spheroids per condition were collected and HA synthesis and pericelular accumulation were determined by flow cytometry (A–C). HA production and accumulation (D red, E) in tumor spheroids were determined by fluorescent microscopy. Nuclei of MDA-MB-231 cells were detected with DAPI (D blue, F). HA production and DAPI staining were compared to spheroids size by correlation analyzes (G–J). Histograms, dotplots and images show the most representative data. Scale bar: 200 μm. Mean ± SEM. *$p < 0.05$, **$p < 0.01$, ***$p < 0.001$, ****$p < 0.0001$.

observed in MCF-7 spheroids under both individual (EPI or 4-MU) and the EPI + 4-MU combined treatments in relation to non-treated spheroids ($p < 0.01$) (Figure 7H). Collectively, these findings indicate that the effect of 4-MU on the expression of enzymes mediating HA synthesis is preserved in the presence of EPI treatment. Furthermore, the marked decrease in UGDH expression, supports the hypothesis that 4-MU enhances the efficacy of EPI by interfering with the production of UDP-GlcUA, a key substrate involved in the inactivation of this cytotoxic drug.

Another critical aspect of tumor ECM dynamics is HA turnover, defined as a delicate equilibrium between its synthesis and degradation. Consequently, we studied the expression of two pivotal hyaluronidases, HYAL-1 and HYAL-2. MDA-MB-231 spheroids exhibited no significant alterations in either HA-specific glycosidase (Figure 7C,D). In contrast, MCF-7 spheroids displayed a distinct response. A significant decrease in HYAL-1 expression was evident across all treatment groups compared to controls ($p < 0.001$) (Figure 7I), although no differential effects among treatments were detected. HYAL-2 expression remained

15216551, 2025, 11, Downloaded from https://iubmb.onlinelibrary.wiley.com/doi/10.1002/iub.70075 by Daiana L. Viale - UNNOBA Uni Nacional del Noroeste de la Provincia de Buenos A , Wiley Online Library on [10/11/2025]. See the Terms and Conditions (https://onlinelibrary.wiley.com/terms-and-conditions) on Wiley Online Library for rules of use; OA articles are governed by the applicable Creative Commons License

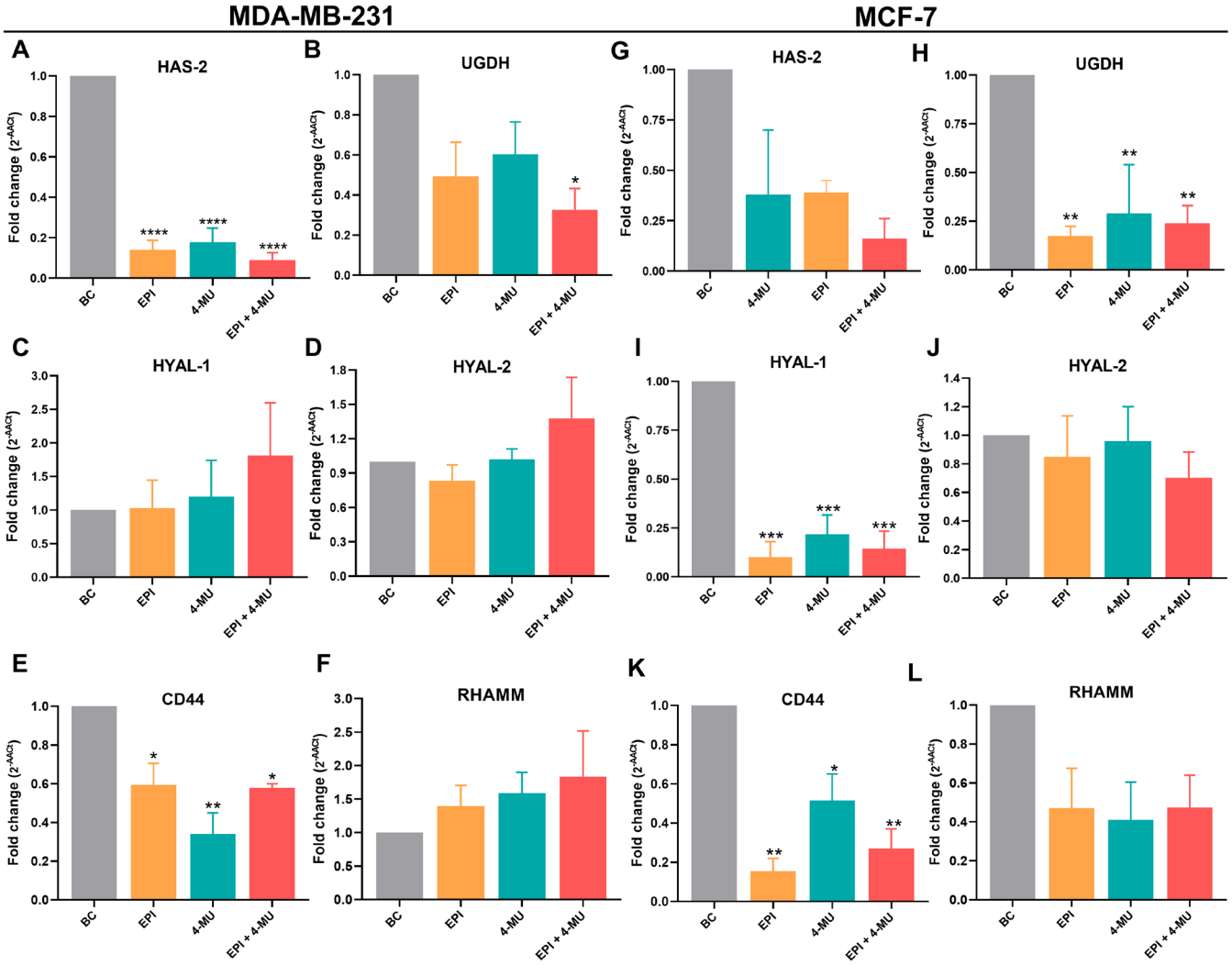


FIGURE 7 | Effect of treatment with EPI in the presence of 4-MU on the expression of HA-related genes. MDA-MB-231 or MCF-7 cells (8×10^3) were cultured under three-dimensional conditions using the hanging drop assay to allow the formation of tumor spheroids. On day 5, the spheroids were treated with 0.5 mM 4-MU plus 1.5 μM EPI (MCF-7) or 0.5 mM 4-MU plus 2.5 μM EPI (MDA-MB-231) for 3 days. On day 8, different spheroids per condition were collected. To evaluate the expression of HA-related genes, total RNA was extracted, and 2 μg were reverse transcribed by RT-PCR. cDNAs were subjected to real time quantitative PCR using SYBR Green. Results were normalized using B2M as reference gene and all determinations were performed as duplicates. $N = 3$, expressed as mean ± SEM. *$p < 0.05$, **$p < 0.01$, ***$p < 0.001$.

unaffected (Figure 7J). These divergent outcomes between the two tumor models may be attributed to the inherent aggressiveness of MDA-MB-231 cells compared to MCF-7.

Finally, a reduction in CD44 levels was observed in MDA-MB-231 spheroids under all treatment conditions compared to controls (EPI $p < 0.05$, 4-MU $p < 0.001$, EPI + 4-MU $p < 0.05$) (Figure 7E), achieving the greatest reduction under 4-MU treatment. Furthermore, this could be related to the modulation of CD44, and HA-mediated pathways involved in cell survival and proliferation, processes that may be affected by EPI + 4-MU treatment. This effect was even more pronounced in MCF-7 spheroids (Figure 7K). Particularly, a decrease in CD44 levels was observed under all treatment conditions when compared to controls (EPI $p < 0.01$, 4-MU $p < 0.05$, EPI + 4-MU $p < 0.01$) (Figure 7F,L). While 4-MU treatment had a negative effect on CD44 expression, treatment with EPI and the combination of both also sustained this decrease. RHAMM expression remained relatively stable across treatments in both cell lines. These findings, combined with the observed reduction in HA synthesis, suggest that 4-MU enhances EPI efficacy not only by increasing drug accumulation but also by modulating the expression of surface receptors that sense specific changes in tumor ECM inhibiting pro-tumor signaling.

2.7 | Effect of 4-MU and EPI Treatment on CD44 Expression

Based on the results obtained from the modulation of CD44 mRNA expression, and considering the relevance of CD44 as a key receptor for HA signaling and a recognized tumor marker, we next analyzed its protein expression in MDA-MB-231 and MCF-7 spheroids by fluorescence microscopy (Figure 8). Since previous analyzes of HA synthesis and accumulation in both spheroid models had ruled out any association between DAPI fluorescence intensity and spheroid size, we quantified CD44 expression relative to DAPI fluorescence

15216551, 2025, 11, Downloaded from https://iubmb.onlinelibrary.wiley.com/doi/10.1002/iub.70075 by Daiana L. Viale - UNNOBA Uni Nacional del Noroeste de la Provincia de Buenos A. , Wiley Online Library on [10/11/2025]. See the Terms and Conditions (https://onlinelibrary.wiley.com/terms-and-conditions) on Wiley Online Library for rules of use; OA articles are governed by the applicable Creative Commons License

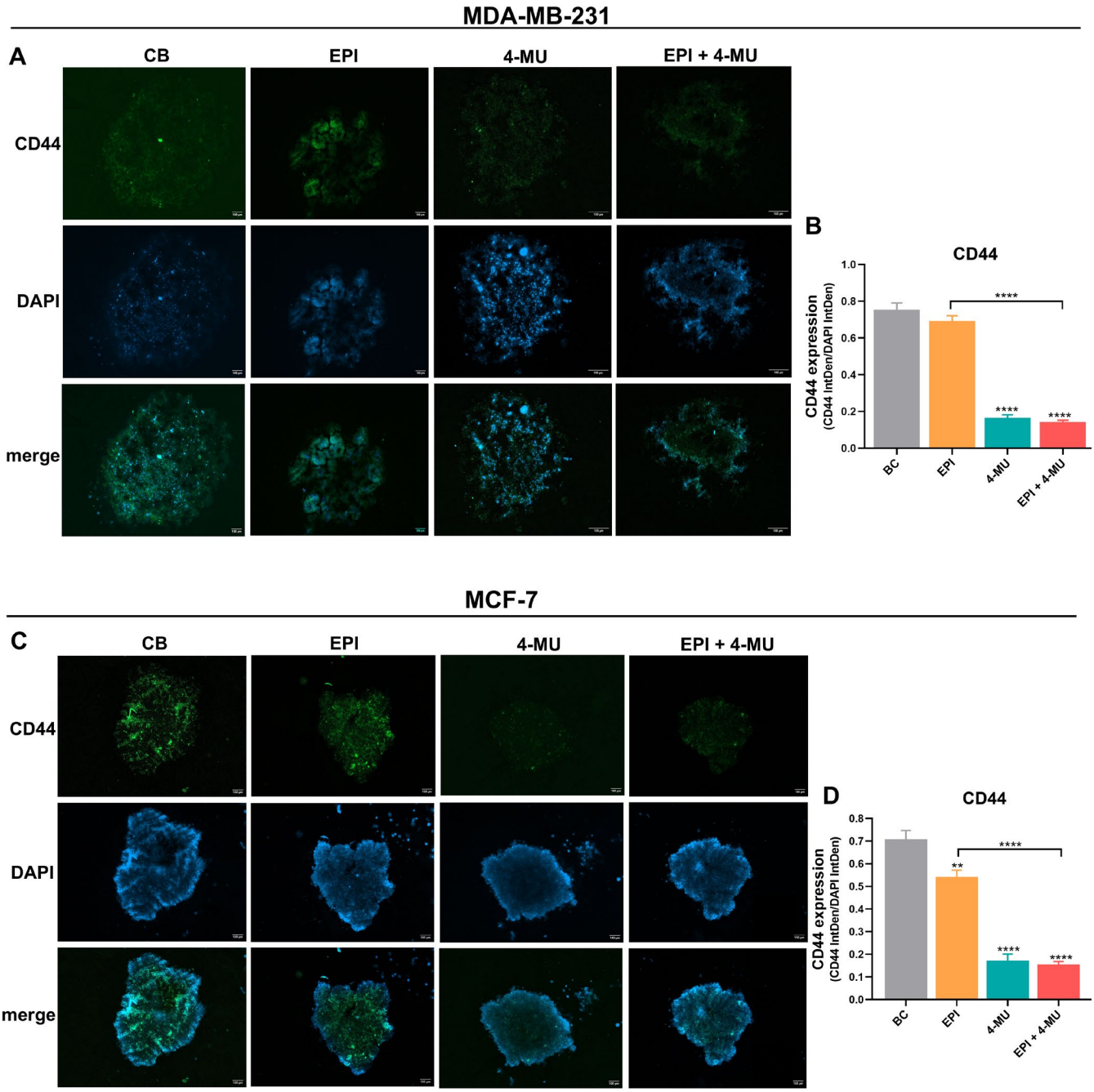


FIGURE 8 | Effect of 4-MU and EPI treatment on CD44 expression in MDA-MB-231 and MCF-7 spheroids. MDA-MB-231 and MCF-7 cells (8×10^3) were cultured under three-dimensional conditions using the hanging drop assay to allow the formation of tumor spheroids. On day 5, the spheroids were treated with 0.5 mM 4-MU plus 1.5 μM EPI (MCF-7) or 0.5 mM 4-MU plus 2.5 μM EPI (MDA-MB-231) for 3 days. On day 8, different spheroids per condition were collected and CD44 expression was determined by fluorescent microscopy (green, A, C). Nuclei of MDA-MB-231 or MCF-7 cells were detected with DAPI (blue, A, C). Bars (B, D) represent the comparison of CD44 expression levels in individual spheroids normalized to DAPI staining. Scale bar: 100 μm. Micrographs show the most representative data. Mean ± SEM. *$p < 0.05$, **$p < 0.01$, ***$p < 0.001$, ****$p < 0.0001$.

to normalize for cell number. Specifically, in MDA-MB-231 spheroids (Figure 8A,B), EPI did not modify CD44 expression compared to BC. This resulted in contrast with the significant downregulation observed at the mRNA level (Figure 7E). Nevertheless, both 4-MU alone and the combined treatment with EPI + 4-MU significantly decreased CD44 protein levels compared to BC ($p < 0.0001$). Notably, the reduction in CD44 levels observed in EPI + 4-MU treatment appeared to be independent of EPI, as it differed significantly from EPI alone ($p < 0.0001$) but not from 4-MU.

Similarly, CD44 protein expression was assessed in MCF-7 spheroids (Figure 8C,D). In this model, EPI treatment significantly reduced CD44 levels compared to the basal condition (BC) ($p < 0.05$), in line with the transcriptional data (Figure 7K). Furthermore, 4-MU and its combination with EPI revealed results comparable to those observed in the MDA-MB-231 spheroids. Specifically, 4-MU markedly decreased CD44 expression relative to BC ($p < 0.0001$), and this reduction was maintained during EPI + 4-MU treatment ($p < 0.0001$). Taken together, these results highlight the

15216551, 2025, 11, Downloaded from https://iubmb.onlinelibrary.wiley.com/doi/10.1002/iub.70075 by Daiana L. Vitale - UNNOBA Uni Nacional del Noroeste de la Provincia de Buenos A. , Wiley Online Library on [10/11/2025]. See the Terms and Conditions (https://onlinelibrary.wiley.com/terms-and-conditions) on Wiley Online Library for rules of use; OA articles are governed by the applicable Creative Commons License

critical role of 4-MU in modulating CD44 expression, particularly when used in combination with EPI, which alone did not achieve such effects—especially in the more aggressive MDA-MB-231 model. Moreover, the consistency between mRNA and protein expression patterns reinforces the validity of CD44 downregulation as a relevant therapeutic readout in response to treatment.

2.8 | Global Impact of 4-MU Treatment on Gene Expression Associated With EPI Response and HA

We aimed to collectively evaluate the gene expression changes associated with EPI + 4-MU treatment and establish potential relationships between these expression changes and the functions of each intermediate. By analyzing the pattern of gene expression in MDA-MB-231 (Figure 9A) and MCF-7 (Figure 9B) spheroids, we observed a difference in the response between the two tumor types. In particular, the ABCC1 pump showed a pattern of increased expression in both tumor models, compared to ABCG2 and ABCC2, which showed a decrease in their expression. The upregulation of RHAMM found in MDA-MB-231 spheroids suggests a possible link to their increased aggressiveness. We continued performing correlation analyzes among all evaluated genes.

First, an analysis of MDA-MB-231 spheroids under different treatments was performed (Figure 9C), where we observed that ABCG2 negatively correlated with RHAMM ($p < 0.05$). In turn, the UGDH enzyme showed a strong and positive relationship with ABCC2 ($p < 0.05$). Furthermore, the changes in HAS-2 expression were shown to be strongly and positively correlated with UGDH and CD44 ($p < 0.05$). However, HAS-2 negatively correlated with RHAMM ($p < 0.05$). This result was expected since RHAMM showed a differential expression pattern in this cell line compared to MCF-7. Finally, as expected, a strong and positive association was observed between HYAL-1 and HYAL 2 ($p < 0.05$). By evaluating the potential interactions between the mediators that resulted in significant correlation in the STRING database, we were able to corroborate that they are functionally and regulatory related (Figure 9E). Forming groups by proximity and close relationship, we observed that a large cluster of functions is associated in this case with HA signaling and metabolism intermediates. Furthermore, CD44, the main HA receptor, was related to ABCG2, a pump mediating EPI expulsion. In turn, the other group is formed with UGDH as a link, grouping certain transferases and enzymes mediating the synthesis of other ECM components not analyzed in this work.

We performed the same correlation analysis of the gene expression data obtained from treated MCF-7 spheroids (Figure 9D). In general, we observed that all the correlations were strong and positive, reflecting the overall lower expression of all analyzed genes under EPI + 4MU treatment. ABCG2 correlated with UGDH ($p < 0.05$), HYAL1 ($p < 0.05$), and RHAMM ($p < 0.01$). On the other hand, HAS-2 showed a strong association with ABCC2, HYAL-1, and UGDH ($p < 0.05$). The UGDH enzyme correlated with HYAL ($p < 0.001$), CD44 ($p < 0.05$), and RHAMM ($p < 0.05$). Finally, HYAL-1 showed a positive and strong association with CD44 and RHAMM ($p < 0.05$). By generating the network of interactions between the cellular effectors that showed correlation (Figure 9F), we observed again a coherent relationship between the evaluated genes, generating two well-separated groups in terms of functionality and regulation. In this case, as observed for MDA-MB-231 spheroids, CD44 acts as a link between the intermediates mediating HA metabolism and drug efflux pumps of the ABC family, highlighting the importance of jointly studying these indicators. Collectively, these results demonstrate that the mitigating effect of 4-MU on HA and other GAGs remains active during EPI treatment, promoting remodeling of the tumor ECM and consequently sensitizing tumor cells to EPI treatment.

2.9 | Synergistic Antitumor Effect of 4-MU and EPI Co-Treatment

Synergy between 4-MU and EPI was analyzed using SynergyFinder 3.0, applying the Highest Single Agent (HSA) method. This model states that the expected combination effect is the maximum of the single drug responses at corresponding concentrations. The combination of 4-MU and EPI resulted in synergy in both MDA-MB-231 (score: 10.356) and MCF-7 (score: 10.171) breast cancer spheroids (Figure 10). While both cell lines showed synergistic responses under the HSA model, the slightly higher score in MDA-MB-231—an aggressive TNBC model—highlights the potential of this combination to target particularly resistant and invasive tumor types. The synergy observed between 4-MU and EPI was particularly significant, as it supports our experimental results showing that 4-MU enhanced the therapeutic efficacy of EPI rather than simply adding its own effect. This interaction goes beyond additivity, as the primary action of 4-MU appears to facilitate the accumulation and effectiveness of EPI in breast cancer cells. Thus, 4-MU firstly enhances the individual effect of EPI by preventing its glucuronidation, thereby increasing its bioavailability and increasing tumor cells' sensitivity. On the other hand, by modulating the ECM and reducing the synthesis of HA, 4-MU may disrupt tumor-associated resistance mechanisms, helping EPI to generate a stronger cytotoxic effect. This is especially relevant in the treatment of aggressive tumor types like TNBC, where chemotherapy remains the mainstay treatment. The ability of 4-MU to potentiate EPI's action opens new possibilities for improving the response to chemotherapy in difficult-to-treat cancers, offering a promising strategy to overcome drug resistance and enhance treatment outcomes.

3 | Discussion

In this work, we proposed to modulate the tumor ECM as a therapeutic target but also to address drug response by altering the intrinsic molecular mechanisms of tumor cells related to the metabolism and inactivation of EPI. Interestingly, the combined treatment with 4-MU and EPI reduced cell viability compared to baseline conditions, highlighting the importance of 4-MU in enhancing the in vitro antitumor efficacy of EPI in both breast cancer models. These findings are consistent with previous studies demonstrating the ability of 4-MU to potentiate the efficacy of another anthracycline, such as doxorubicin [17]. While these precedents provided an important foundation for this study, the proposed approach did not consider the use of EPI

15216551, 2025, 11, Downloaded from https://iubmb.onlinelibrary.wiley.com/doi/10.1002/iub.70075 by Daiana L. Viale - UNNOBA Uni Nacional del Noroeste de la Provincia de Buenos A. , Wiley Online Library on [10/11/2025]. See the Terms and Conditions (https://onlinelibrary.wiley.com/terms-and-conditions) on Wiley Online Library for rules of use; OA articles are governed by the applicable Creative Commons License

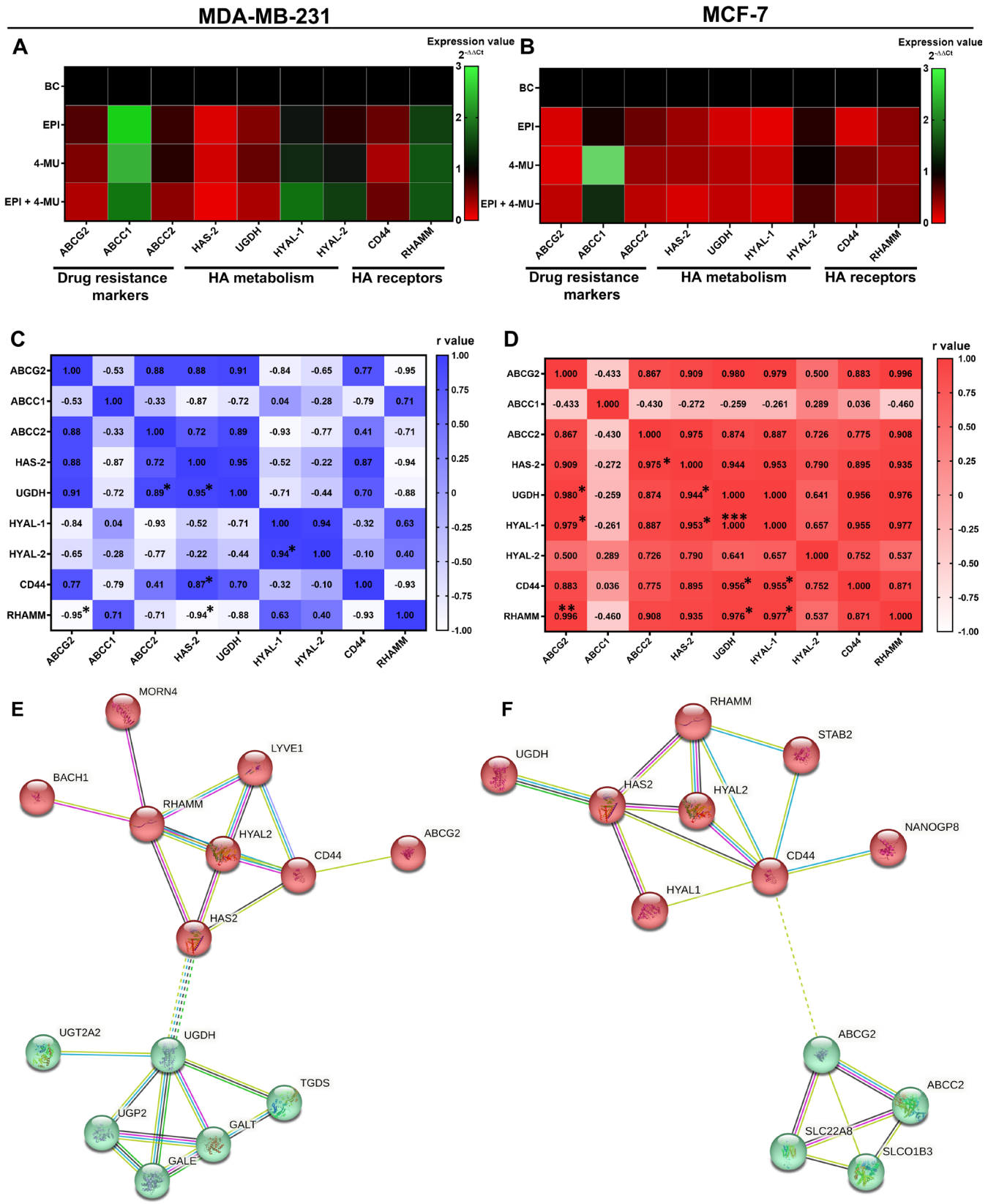


FIGURE 9 | Global impact of 4-MU treatment on gene expression associated with EPI response and HA. Analysis of gene expression changes related to drug resistance, HA metabolism, and its main receptors in MDA-MB-231 (A) or MCF-7 (B) treated spheroids. The results are shown as a heat map with $2^{-\Delta\Delta Ct}$ values. Correlation analysis of colorectal and breast cancer markers. The results of correlation analysis for MDA-MB-231 (C) or MCF-7 (D) are shown as a heat map with *r* values. All *r* values above 0.8 (or under −0.8) were considered a strong correlation and *p*-values lower than 0.05 were considered statistically significant. STRING database output depicting functional and physical interactions between the evaluated interactors associated with MDA-MB-231 (E) and MCF-7 (F) cells, obtained from http://string-db.org/. $*p < 0.05$, $**p < 0.01$, $***p < 0.001$, $**p < 0.0001$.

15216551, 2025, 11, Downloaded from https://iubmb.onlinelibrary.wiley.com/doi/10.1002/iub.70075 by Daiana L. Viale - UNNOBA Uni Nacional del Noroeste de la Provincia de Buenos A., Wiley Online Library on [10/11/2025]. See the Terms and Conditions (https://onlinelibrary.wiley.com/terms-and-conditions) on Wiley Online Library for rules of use; OA articles are governed by the applicable Creative Commons License

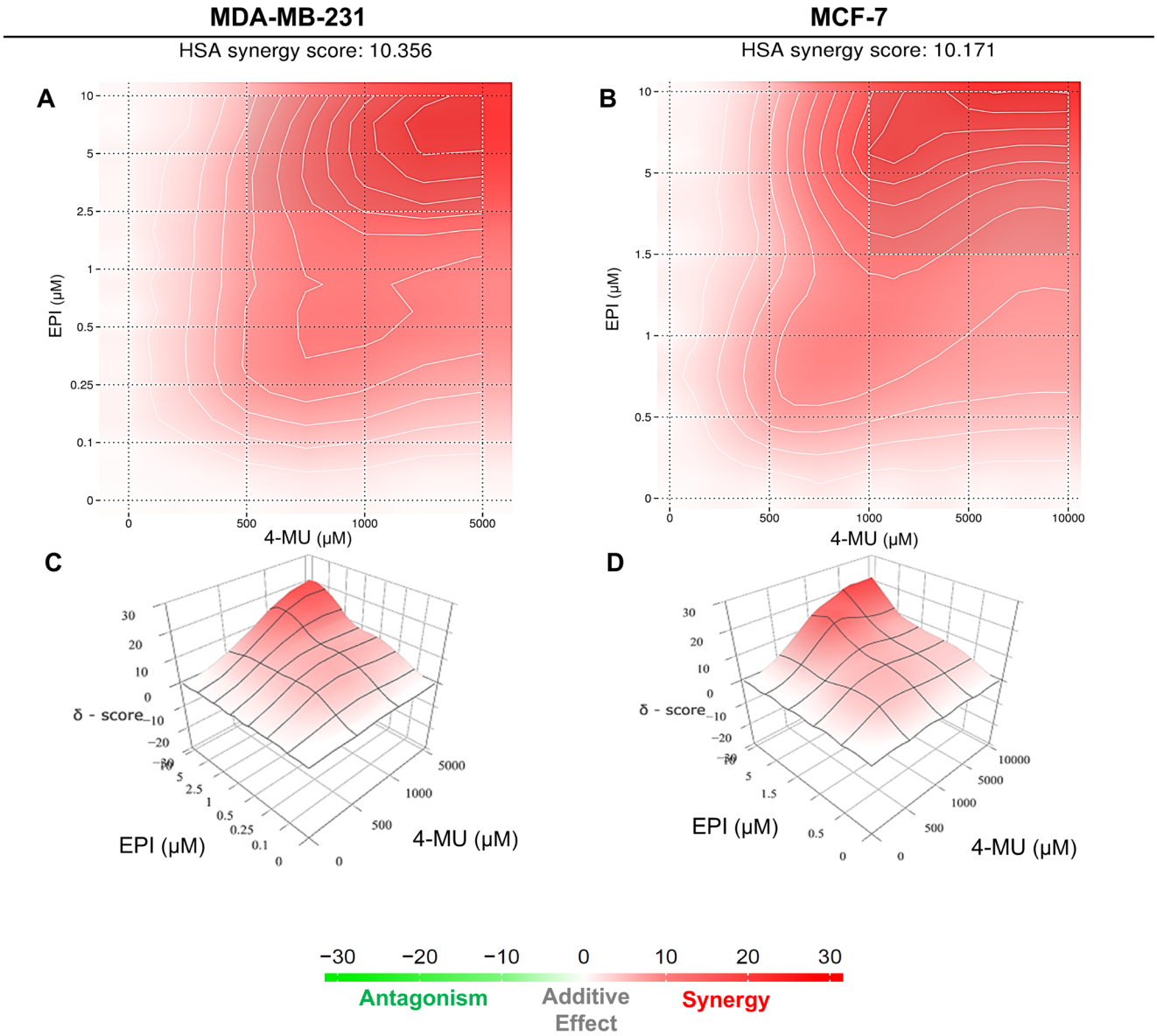


FIGURE 10 | Synergy effect between EPI and 4-MU. MDA-MB-231 and MCF-7 spheroids were treated with different concentrations of EPI and 4-MU for 3 days and cell viability was determined by MTS. Synergy was calculated using SynergyFinder 3.0, employing the HAS method. Synergy plots (A, B) and isobolograms (C, D) show the occurrence of synergy (red), addition (white), or antagonism (green) of the different combinations of EPI and 4-MU concentrations for both tumor spheroids. A score of −10 or lower indicates antagonism, −10 to 10 indicates additivity, and a score of 10 or greater is synergy (https://synergyfinder.fimm.fi/).

as another target of action for 4-MU, in addition to modulating the tumor ECM.

When assessing cell viability in the MCF-7 model, an undesirable effect was observed, as treatment with 4-MU alone reduced viability compared to control spheroids. This result prompted additional experiments to rule out potential toxic effects, particularly on this cell type. Given their distinct phenotype compared to MDA-MB-231 cells, MCF-7 cell-ECM adhesion markers and HA differ from MDA-MB-231 cells [18–20]. Therefore, affecting the ECM with the addition of 4-MU could make MCF-7 cells more susceptible to changes in spheroid formation and potentially impact their proliferation and viability. Cytotoxicity assays revealed no significant differences in LDH enzyme activity released into the supernatants of MDA-MB-231 and MCF-7 spheroids. This result allowed us to rule out significant toxic effects at the cellular and extracellular levels caused by 4-MU and EPI. Moreover, the cytotoxicity levels similar to control conditions indicated that the EPI + 4-MU treatment could affect cell viability without inducing the release of cellular content into the external environment, potentially preventing inflammatory or cytotoxic conditions. Furthermore, the lack of detected cytotoxicity is consistent with studies reporting that 4-MU does not produce direct cytotoxic effects on tumor cells [21]. However, there is one report suggesting that while 4-MU acts as an antioxidant and antimicrobial agent in the circulatory system, it may exert toxic effects on hemocytes and hematopoiesis. Nevertheless, this study was conducted in a different pathophysiological context, with higher doses of 4-MU and in invertebrate animals [22], which is far from our study model. On the other

15216551, 2025, 11, Downloaded from https://iubmb.onlinelibrary.wiley.com/doi/10.1002/iub.70075 by Daiana L. Viale - UNNOBA Uni Nacional del Noroeste de la Provincia de Buenos A , Wiley Online Library on [10/11/2025]. See the Terms and Conditions (https://onlinelibrary.wiley.com/terms-and-conditions) on Wiley Online Library for rules of use; OA articles are governed by the applicable Creative Commons License

hand, the reduction in tumor cell viability without inducing cytotoxic effects may be attributed to a potential cytostatic effect of our proposed treatment. This effect could primarily be due to EPI, which, as a DNA intercalator, induces molecular damage that affects cell proliferation [23, 24]. Furthermore, it has been shown that 4-MU exhibits antiproliferative properties in cancer context [25]. Therefore, the observed effect of the combined EPI and 4-MU treatment may be mediated by a cytostatic mechanism, which will be further investigated in future studies.

We acknowledge the critical importance of evaluating the potential toxicity of EPI and 4-MU co-treatment in non-tumoral cells, a fundamental aspect of its preclinical development. In this sense, EPI has been shown to exert cardiotoxic effects in human cardiac myocytes, with significant toxicity observed at concentrations starting from 2.5 μM after prolonged exposure [26]. It is important to note that the concentrations of EPI used in our study, and the short-term exposure are below the threshold considered acutely cytotoxic. This finding suggests a potentially safer therapeutic window for our combination treatment. In contrast, 4-MU exhibits low toxicity toward normal cells at concentrations that inhibit tumor cell growth or HA synthesis. For example, primary human hepatocytes were unaffected under conditions where hepatocellular carcinoma cells underwent growth inhibition and apoptosis, and normal fibroblasts display higher lethal thresholds than tumor counterparts [27]. Endothelial cell assays also indicate that cytotoxicity emerges only at relatively high millimolar doses [28]. These preclinical findings align with human studies showing that 4-MU is generally safe and well tolerated [29, 30].

Nevertheless, systemic inhibition of HA synthesis with 4-MU may affect HA-dependent functions in normal tissues, such as joint lubrication, skin hydration, and airway or vascular glycocalyces. Clinical experience and trials indicate a generally favorable safety profile, with dose-dependent gastrointestinal events, mainly diarrhea (1%–10%), being the most common adverse effects [31]. A Phase 1 study in healthy adults demonstrated that short-course oral 4-MU reduced sputum HA and was well tolerated at the tested doses [30], and more recent randomized studies in other indications also report acceptable tolerability under medical supervision [32]. Nevertheless, on-target effects on the endothelial glycocalyx and vascular homeostasis have been observed in animal models with systemic HA suppression, highlighting the need for careful dose selection and monitoring. Future translational strategies could consider tumor-targeted, intermittent, or nanoparticle-based delivery to mitigate potential off-tumor effects [33].

When analyzing the potential changes in EPI accumulation, MDA-MB-231 spheroids showed higher aggressiveness compared to MCF-7 model, related with its intrinsic features [18]. Nonetheless, in both tumor contexts, 4-MU significantly enhanced EPI access and accumulation compared to treatment with EPI alone. Specifically, MDA-MB-231 spheroids treated with EPI + 4-MU showed an increase in the number of EPI+ cells and EPI accumulation per cell, whereas MCF-7 spheroids only exhibited an increase in the percentage of cells containing the drug. These results suggest that 4-MU improves EPI uptake within tumor spheroids through a dual mechanism. First, the increase in the number of EPI+ cells, that is, cells that managed to incorporate the drug, could be associated with the direct effect of 4-MU on HA synthesis and, consequently, on the tumor ECM. This may result in reduced HA accumulation and a less dense tumor ECM, allowing the drug to reach a greater number of tumor cells that could not be accessed without 4-MU treatment. Second, the increased EPI uptake per cell also suggests an effect on metabolism and inactivation of EPI. 4-MU may act by increasing EPI retention within tumor cells due to the sequestration of GlcUA required for its inactivation and expulsion [34, 35]. The increase in intracellular EPI accumulation in the presence of 4-MU is consistent with studies showing that ECM modulation can enhance drug penetration and retention in solid tumors, such as breast cancer, thereby improving treatment efficacy.

Moreover, it is important to note that the increased penetration and accumulation of EPI in cells derived from both types of spheroids were associated with a higher antitumor efficacy of EPI compared to treatment without 4-MU. Specifically, an increase in the percentage of apoptotic cells containing EPI was observed in the presence of 4-MU in both tumor models. This suggests that the incorporation and accumulation of EPI effectively translate into increased sensitivity. In parallel, the analysis of the activation of caspase 3 revealed that the combination of EPI + 4-MU significantly increased the proportion of apoptotic cells in the TNBC model. This effect appeared to be synergistic, as treatment with EPI or 4-MU alone did not significantly differ from the basal conditions. Nevertheless, no significant differences were found in the expression levels of cleaved caspase-3 per cell, as measured by MFI. These findings strongly suggest that the observed effects on increased apoptosis induction are likely mediated through modulation of ECM. By inhibiting HA synthesis, 4-MU reduces ECM density which could alter the structural composition of the spheroids´ stroma and improve drug penetration into deeper spheroid layers [36, 37], enhancing the overall cytotoxic efficacy of EPI. Even more, it has been demonstrated that degradation of HA in oligomers suppress PI3K/AKT pathway in murine mammary and human colon carcinoma cells, leading to the activation of pro-apoptotic mediators, and increased activity of the caspase-3 [38].

This phenomenon was particularly pronounced in the MDA-MB-231 model, highlighting again the differences between the two tumor models. However, it is worth noting that both tumor types represented by the spheroids became more sensitive relative to their control conditions, in both annexin V and CC3 assays. Similarly, several studies have shown that affecting HA metabolism sensitizes tumor cells to chemotherapy, which aligns with our results in breast cancer. Furthermore, it has been demonstrated that inhibiting HA synthesis with 4-MU sensitizes prostate cancer cells to doxorubicin therapy [39]. Additionally, it was found that 4-MU treatment reduced resistance to paclitaxel in ovarian cancer cells [40], similarly reducing resistance to temozolomide in glioblastoma cells. These studies contribute to understanding how HA and a dense ECM contribute to treatment resistance by creating a physical barrier that impedes the proper distribution and accumulation of chemotherapeutic drugs [41].

To further investigate the sensitization to EPI treatment due to 4-MU, we studied the ABC family pumps involved in the efflux

15216551, 2025, 11, Downloaded from https://iubmb.onlinelibrary.wiley.com/doi/10.1002/iub.70075 by Daiana L. Viale - UNNOBA Uni Nacional del Noroeste de la Provincia de Buenos A. , Wiley Online Library on [10/11/2025]. See the Terms and Conditions (https://onlinelibrary.wiley.com/terms-and-conditions) on Wiley Online Library for rules of use; OA articles are governed by the applicable Creative Commons License

of anthracyclines such as EPI [42, 43]. These transporters have been extensively studied based on their expression levels as biomarkers of therapeutic response, aggressiveness, and drug resistance, highlighting their potential as modulable targets in cancer therapy [44, 45]. Moreover, various studies have linked HA and its interaction with its primary receptor (CD44) to the expression and functionality of different transporters of this family in cancer, such as ABCB1 (or P-glycoprotein) [46], ABCC3 (or MRP2) [47], ABCG2 (or BCRP) [48], and ABCC2 [49]. In particular, the PI3K/AKT signaling pathway, involved in cell survival and proliferation, has been suggested as the central intracellular axis driving the expression of these drug efflux pumps due to the HA-CD44 interaction [25, 50]. The reduction of ABCG2 and ABCC2 expressions during EPI + 4-MU treatment was consistent with the differential accumulation of EPI observed during co-treatment with 4-MU. This result suggests not only transcriptional regulation but also a potential functional impact on ABC pumps. The increased intracellular accumulation of EPI observed during 4-MU treatment may be attributed also to the decreased expression of these transporters and their ability to expulse chemotherapeutic drugs as EPI, potentially resulting in reduced chemotherapy resistance. Even more, these results were in line with studies demonstrating that inhibiting HA synthesis can alter the regulation of genes associated with multidrug resistance, including ABC family pumps [51]. Given the therapeutic goal of reducing tumor mass during chemotherapy treatment, we conducted individual monitoring of spheroid size throughout the culture period and treatments. In untreated MDA-MB-231 spheroids, an expected increase in size was observed, which could mimic tumor growth without treatment. This highlights the importance of using three-dimensional models to study drug resistance and tumor progression [52]. On the other hand, considering pre and posttreatment size, the combination of EPI + 4-MU was the only treatment that resulted in a significant reduction in spheroid size compared to the control group, highlighting the importance of combined treatment to reduce tumor size in this aggressive model. MCF-7 spheroids were shown to be more sensitive to EPI treatment, since EPI treatment diminished spheroids size, an effect that was similar during the combined treatment with 4-MU. While there were differences in the observed response during the analysis of both tumor models, it is noteworthy that both responded more effectively to the combination of EPI + 4-MU compared to individual treatments and untreated conditions. This could be due to intrinsic differences in ECM composition between the two cell types, which warrants further investigation.

The reduction in HA levels from cells derived from 4-MU-treated spheroids corroborates the ability of 4-MU to reduce HA synthesis even in a three-dimensional model after 3 days of treatment. This supports the previous hypothesis of the dual effect of 4-MU on EPI treatment, where a reduction in HA content in the tumor ECM could improve EPI efficacy by facilitating its access to the tumor cells within the spheroid. This is also supported by numerous studies that have discussed how the density of HA in the ECM can act as a physical barrier preventing the penetration of chemotherapeutic agents in various tumor types [51, 53]. Additionally, the characterization of cell populations based on EPI accumulation and HA synthesis reveals that combined treatment with 4-MU and EPI not only affect HA synthesis but also alters the distribution and organization of cells within the spheroid.

Our findings also demonstrated that treatment with 4-MU and EPI had a significant impact on the regulation of HA metabolism. As previously reported by several authors [14, 16, 21, 54], treatment with 4-MU alone led to a decrease in the expression of HAS2. This was crucial to determining that the regulation of HA synthesis could also be affected during combined treatment with EPI, and to highlight the relevance of the effect of 4-MU being maintained in a three-dimensional context. As reported by other authors, the modulation of HAS2 expression by 4-MU was related to ER expression [55]. The inhibitory effect on synthase expression was more evident in MDA-MB-231 cells, which lack ER expression, compared to the effect observed in MCF-7 cells, which express this receptor. Furthermore, the decrease in UGDH expression was particularly notable, supporting the hypothesis that 4-MU enhances EPI efficacy by interfering with the production of GlcUA, a key substrate for glucuronidation and eventual inactivation of EPI. Additionally, considering that UGDH is regarded as a potential poor prognostic marker in oncology and a therapeutic target in cancer biology [56–58], a reduction in its expression could also indicate increased sensitivity to treatment.

The differential behavior observed between MDA-MB-231 and MCF-7 spheroids with respect to HYAL expression was an intriguing finding. In MDA-MB-231 spheroids, there was a trend toward increased expression of HYAL-1 and HYAL-2 after combined treatment with EPI and 4-MU. This phenomenon could represent a compensatory mechanism in response to decreased HA synthesis, as HYALs may contribute to ECM remodeling and, in some cases, promote tumor progression [59]. This compensatory behavior may be particularly relevant in more aggressive tumor models, such as MDA-MB-231, where the ECM plays a crucial role in invasion and treatment resistance. In contrast, the significant decrease in HYAL-1 expression in MCF-7 spheroids across all treatments indicates a different response that may be related to the lower aggressiveness of this cell model. Several authors have highlighted that differences in HYAL regulation among various tumor types may be associated with tumor aggressiveness and invasive capacity [60–63], which could explain the variations observed between MDA-MB-231 and MCF-7 in our study.

The modulation of CD44 and RHAMM receptor expression by the treatments also shed light on the underlying mechanisms of the tumor response. We observed a reduction in CD44 expression in MDA-MB-231 spheroids following 4-MU treatment, consistent with studies showing the involvement of CD44 in tumor progression and chemotherapy resistance and further highlighting its role as a cancer stem cell marker [43, 64]. Importantly, the reduction in CD44 protein levels observed in both spheroid models during the EPI + 4-MU co-treatment appeared to be driven primarily by 4-MU, as it differed significantly from EPI treatment alone but not from 4-MU alone. Notably, in MCF-7 spheroids, EPI treatment by itself also significantly reduced CD44 protein expression compared to basal conditions, consistent with the transcriptional findings. Taken together, these results underscore the central role of 4-MU in modulating CD44 expression and further highlight the pronounced sensitivity of

15216551, 2025, 11, Downloaded from https://iubmb.onlinelibrary.wiley.com/doi/10.1002/iub.70075 by Daiana L. Viale - UNNOBA Uni Nacional del Noroeste de la Provincia de Buenos A , Wiley Online Library on [10/11/2025]. See the Terms and Conditions (https://onlinelibrary.wiley.com/terms-and-conditions) on Wiley Online Library for rules of use; OA articles are governed by the applicable Creative Commons License

the MCF-7 model to EPI treatment, especially when compared to the more aggressive MDA-MB-231 cells. Therefore, reduced CD44 expression could be associated with decreased ability of tumor cells to interact with their environment, leading to reduced proliferation and resistance to EPI. RHAMM has been widely studied in conjunction with CD44 in cell migration and cytoskeleton organization, suggesting that tumor cells may attempt to compensate for the loss of CD44 by overexpressing RHAMM [65]. This compensatory phenomenon could be particularly relevant in treatment contexts where normal cell-ECM interactions are disrupted, especially in more aggressive tumors like TNBC, which are less responsive to therapy.

Our results confirm the effectiveness of 4-MU in reducing HA synthesis in a three-dimensional context through the study of changes in HA synthesis and accumulation in the ECM of spheroids. Fluorescence microscopy analysis confirmed these findings, showing a marked reduction in HA production following 4-MU treatment, both in the absence and presence of EPI. This suggests that the effect of 4-MU on HA synthesis persists even under co-treatment with EPI, similar to the results observed when studying HAS-2 expression. A key aspect of our results is the lack of correlation between HA content and the physical dimensions of the spheroids, such as area and perimeter. This indicates that the observed decrease in HA synthesis is not simply a side effect of spheroid size reduction but a direct result of 4-MU's action on the HA biosynthetic machinery [66].

In addition to the direct effect on breast cancer cells demonstrated in our study, it is crucial to consider the impact of EPI on other associated cells of the TME. In this sense, cancer-associated fibroblasts (CAFs) are recognized as the principal architects of the tumor stroma and a primary source of HA [67, 68]. Therefore, the possibility that EPI, in addition to its cytotoxic action on tumor cells, may also produce an effect on CAFs is a hypothesis of great therapeutic relevance. Such modulation of the stromal compartment could disassemble the pro-tumoral and chemoresistant niche, sensitizing the tumor to treatment. Although our current experiments do not directly evaluate the response of CAFs, this intriguing possibility highlights a new dimension in the mechanism of action of EPI and underscores the importance of targeting therapies not only at the cancer cell but also at the components of the microenvironment that sustain it [69, 70]. Indeed, mesenchymal stromal cells are another key factor in the TME, which have been shown to confer doxorubicin resistance in breast cancer by diminishing its intratumoral accumulation. This chemoresistant effect was mediated by HA, as evidenced by its abrogation upon depletion or inhibition of HAS2 [71].

Finally, the combination of EPI with 4-MU not only enhanced drug accumulation in spheroids but also altered the composition of the ECM, facilitating drug penetration and modifying the profile of cell populations found within the tumor spheroids. Based on the synergy model used, 4-MU generates a synergistic effect when combined with EPI enhancing the individual effect of EPI by preventing its glucuronidation, thereby increasing its bioavailability and increasing tumor cells' sensitivity. This increased sensitivity of tumor cells may indeed be reflected in the expression of progression and resistance markers we analyzed. On the other hand, by modulating the ECM and reducing the synthesis of HA, 4-MU may also disrupt resistance mechanisms mediated by ECM, improving EPI to generate a stronger cytotoxic effect. The observed synergy between these drugs suggests that targeting multiple molecular pathways can significantly improve treatment efficacy and overcome drug resistance, avoiding the need for more aggressive and cytotoxic doses. The implementation of this therapeutic combination in clinical trials could revolutionize current treatment guidelines, reducing not only the side effects associated with aggressive therapies but also the cost of care for patients with limited resources. Thus, our study establishes a solid precedent for continuing in vivo evaluation of this therapeutic combination, paving the way for transitioning from preclinical models to clinical trials. With these findings, we propose a new therapeutic paradigm that not only increases response rates in breast cancer but also aligns with principles of accessibility and health equity, offering a promising strategy to overcome drug resistance and enhance treatment outcomes.

4 | Conclusions

The results obtained in this study demonstrate that the therapeutic combination of EPI and 4-MU is significantly more effective in treating two three-dimensional breast cancer models compared to individual treatments. Specifically, the presence of 4-MU during EPI chemotherapy was able to reduce cell viability and promote the death of MDA-MB-231 and MCF-7 spheroids compared to treatment with EPI alone. Furthermore, the combination increased the intracellular accumulation of EPI in tumor cells, facilitating the drug's access to previously inaccessible cells. This effect was accompanied by a decrease in the expression of efflux pumps, suggesting an improvement in treatment efficacy without the need to increase the indicated dose, thereby reducing the risk of toxicity. Additionally, 4-MU showed a significant diminishing effect on the synthesis, metabolism, and accumulation of HA in the tumor ECM, which could contribute to the reduction in spheroid size and compaction. Moreover, this inhibitor also demonstrated an effect at the spheroid level, preventing the activation of pro-tumor signals typical of an HA-rich environment.

Finally, these findings underscore the importance of repositioning already approved drugs, such as EPI and 4-MU, as a promising therapeutic strategy for the treatment of breast cancer, regardless of the molecular phenotype each tumor presents. The observed synergy between these drugs suggests that by targeting multiple molecular pathways, treatment efficacy can be significantly improved, overcoming drug resistance. This not only enhances treatment efficacy but also facilitates equitable access to effective therapies in regions with limited resources, where exhaustive molecular characterization and personalized therapies are not available. This study establishes a solid foundation for the in vivo evaluation of this therapeutic combination, laying the groundwork for its potential clinical implementation.

5 | Methods

5.1 | Cell Lines Culture

Human breast cancer cell lines with well-differentiated molecular profiles were used. The MDA-MB-231 cell line (ATCC HTB-26) was chosen to represent TNBC, which represents

15216551, 2025, 11, Downloaded from https://iubmb.onlinelibrary.wiley.com/doi/10.1002/iub.70075 by Daiana L. Viale - UNNOBA Uni Nacional del Noroeste de la Provincia de Buenos A. Wiley Online Library on [10/11/2025]. See the Terms and Conditions (https://onlinelibrary.wiley.com/terms-and-conditions) on Wiley Online Library for rules of use; OA articles are governed by the applicable Creative Commons License

greatest treatment challenges, and EPI is commonly used for its treatment [72]. Additionally, the MCF-7 cell line (ATCC HTB-22) was used to represent the luminal phenotype. This breast cancer type is more frequent and less aggressive than the TNBC [73, 74]. Both cell lines were maintained in DMEM-high glucose medium supplemented with 2 mM L-glutamine, 100 IU penicillin, 100 μg/mL streptomycin and 10% v/v of fetal bovine serum (FBS) in a humidified incubator at 37°C and 5% CO_2. During all cell cultures, periodic checkups of cell morphology and growth rate were performed, in addition to strict control of cell line passages. Cell lines were also analyzed to discard the presence of mycoplasma contamination by PCR.

5.2 | Tridimensional Cell Culture: Hanging Drop Assay

For spheroids formation in hanging drops, a suspension of 400,000 cells/mL from each cell line was prepared. Then, 20 μL drops containing 8000 cells were displayed on the upper side of Petri dishes, which were incubated for 5 days with complete growth medium in a humidified atmosphere of 5% CO_2 at 37°C to allow the correct formation of the spheroids.

5.3 | EPI and 4-MU Treatments

Epirubicin (EPI) was purchased from Selleckchem. 4-methylumbelliferone (4-MU) sodium salt was purchased from Sigma-Aldrich. The dose of EPI for each tumor model was determined by calculating the half maximal inhibitory concentration (IC_{50}) dose from spheroids treated with a range of EPI concentrations. A dose of 1.5 μM EPI for MCF-7 cells and 2.5 μM of EPI for MDA-MB-231 cells were selected. The dose of 4-MU (0.5 mM) for both tumor spheroids was selected considering previous results of our laboratory and to avoid cytotoxic effects (*data not shown*). Spheroids from both cell lines were seeded as previously described (day 0). After 5 days of hanging drop culture (day 5), MDA-MB-231 and MCF-7 spheroids were treated with EPI, 4-MU, or a combination of both (EPI + 4-MU) for 3 days, resulting in a total culture period of 8 days (day 8). Fresh culture medium was prepared containing the required amounts of EPI, 4-MU, or both drugs (EPI + 4-MU) to achieve the desired doses in a final volume of 20 μL. Untreated spheroids served as basal controls (BC) and received fresh culture medium on day 5. The initial number of spheroids varied depending on the subsequent assay.

5.4 | Evaluation of Spheroid Integrity After Dissociation and Re-Plating

For the experiments that required spheroid dissociation, we applied a gentle mechanical protocol designed to preserve cell integrity and minimize mechanical stress. Spheroids were gently dissociated using a mechanical protocol consisting of controlled vortexing and repeated pipetting to minimize cell damage while ensuring efficient disaggregation into single-cell suspensions. Representative bright-field images of dissociated MDA-MB-231 and MCF-7 spheroids are shown in Figures S1A and S2A, respectively. To further assess spheroid integrity and the potential to continue cell-based assays after treatments, individual spheroids from each condition were re-plated onto solid gelatin-coated supports and cultured for 48 h. This approach allowed evaluation of posttreatment adhesion and spreading capacity as indicators of cell viability and structural preservation (Figures S1B and S2B).

5.5 | Viability Assay

MDA-MB-231 and MCF-7 spheroids were formed and treated with EPI and 4-MU as described previously. On day 8, four representative spheroids from each condition were mechanically homogenized and seeded into a 96-well plate containing 100 μL of fresh culture medium and 7 μL of MTS Reagent (Abcam). Each treatment was performed with three technical replicates (12 spheroids of each condition). The cells were incubated at 37°C and 5% CO_2 for 4 h. Optical density (OD) was measured using the spectrophotometer iMark (Bio-Rad Laboratories) at 490 nm.

5.6 | Cytotoxicity Assay

Cytotoxicity was evaluated by measuring the activity of lactate dehydrogenase (LDH) released from damaged cells using the LDH Cytotoxicity Assay Kit (Abcam). The LDH enzyme oxidizes lactate to pyruvate, which reacts with tetrazolium salt (INT) to form formazan. Each treatment was performed with four technical replicates. Supernatants from MDA-MB-231 and MCF-7 spheroids of each condition were analyzed according to the manufacturer's protocol.

5.7 | Apoptosis Detection Assay

MDA-MB-231 and MCF-7 spheroids were treated as detailed before. On day 8, 50 spheroids of each condition were mechanically homogenized, washed, and marked with annexin V-FITC (Novus Biologicals) for 30 min at room temperature (RT) according to the manufacturer's protocol. Samples were analyzed using a FACS Canto II cytometer (BD Biosciences) and results were evaluated using FlowJo 5 software (BD Biosciences). The gating strategy applied to all FACS analyzes is summarized in Figure S3, showing representative examples of the sequential gating steps used to identify single cells and ensure consistency across all experimental conditions.

5.8 | Determination of Intracellular Accumulation of EPI

EPI is a small molecule capable of emitting fluorescence detectable by flow cytometry (550–600 nm). This property enables the determination of intracellular EPI accumulation, as previously described [75]. On day 8, 50 MDA-MB-231 and MCF-7 spheroids treated with EPI or EPI + 4-MU were mechanically homogenized and washed with PBS. EPI fluorescence was collected using a 564–606 nm band-pass filter on a FACS Canto II cytometer (BD Biosciences). Data was analyzed using FlowJo 5 software (BD Biosciences).

15216551, 2025, 11, Downloaded from https://iubmb.onlinelibrary.wiley.com/doi/10.1002/iub.70075 by Daiana L. Viale - UNNOBA Uni Nacional del Noroeste de la Provincia de Buenos A. , Wiley Online Library on [10/11/2025]. See the Terms and Conditions (https://onlinelibrary.wiley.com/terms-and-conditions) on Wiley Online Library for rules of use; OA articles are governed by the applicable Creative Commons License

5.9 | Intracellular Flow Cytometry for Detection of Cleaved Caspase-3

To evaluate apoptosis induction, intracellular staining of cleaved caspase-3 was performed by flow cytometry. Briefly, on day 8, 50 MDA-MB-231 spheroids treated with EPI or EPI + 4-MU were mechanically homogenized and fixed with 4% paraformaldehyde (PFA). After washing, cells were permeabilized using a saponin-based buffer (0.5% saponin in PBS containing 10% FBS) to allow intracellular antibody access. Staining was performed using a primary anti-cleaved caspase-3 antibody (1:800, Asp175, #9661, Cell Signaling Technology) followed by a secondary anti-mouse antibody conjugated to Alexa Fluor 488 (AF488, 1:500, Cell Signaling). Samples were analyzed on a FACS Canto II flow cytometer (BD Biosciences), and data were processed using FlowJo software (BD Biosciences). The percentage of cleaved caspase-3-positive cells (CC3+) and mean fluorescence intensity (MFI) were calculated for each condition (Figure S4).

5.10 | RNA Extraction and cDNA Synthesis

Total RNA was extracted from MDA-MB-231 and MCF-7 spheroids using Tri Reagent (MRC). On day 8, 120 spheroids of each condition were collected in 500 μL of Tri Reagent. Total RNA was obtained following the manufacturer's protocol. RNA integrity and quantification were assessed spectrophotometrically by measuring OD260 and OD280 using a Picodrop instrument. Reverse transcription of mRNA (1 μg) into cDNA was performed by reverse transcriptase PCR (RT-PCR) using a Veriti thermocycler (Applied Byosystems). The RT-PCR reaction mixture contained 2 μg of total RNA, 100 pmol/μL of oligos (dT) (Genbiotech), 10 mM dNTPs (Genbiotech) and 100 U of M-MLV reverse transcriptase (Promega).

5.11 | Quantitative Real-Time PCR

qPCR for each gene was performed using Sso Advanced Universal SYBR Green Supermix (Bio-Rad Laboratories) containing 200 nM of each specific primer. Gene expression was quantified with the CFX96 Touch Real-Time PCR Detection System (Bio-Rad Laboratories). The amplification conditions were as follows: 30 s at 95°C, followed by 40 cycles of 15 s at 95°C and 30 s at 60°C. The $2^{-\Delta\Delta Ct}$ method was used for the transcriptional analysis, and target gene expression was normalized to β2M expression levels. Primer sequences were confirmed by NCBI BLAST analysis and are provided in the Table S1.

5.12 | Determination of Tumor Spheroids Size

The final perimeter and volume of MDA-MB-231 and MCF-7 spheroids were measured on day 8. Micrographs of at least eight spheroids were captured with a digital camera (Infinity 3-Lumenera) coupled to an inverted optical microscope (Carl Zeiss). To determine potential changes pre and post treatment, micrographs of individually selected spheroids from each condition were taken on day 5 (pretreatment) and day 8 (post-treatment) to calculate its area. The area and perimeter were determined using ImageJ (NIH). To calculate the volume, the ellipsoid formula was applied, adjusting the calculation for non-spherical spheroids, as previously described [76].

5.13 | Determination of HA Single-Cell Coat by Flow Cytometry

HA pericellular accumulation was detected by flow cytometry as previously described [77]. Briefly, on day 8, 50 spheroids of each condition were mechanically homogenized, washed, and labeled with a HA-binding protein conjugated to biotin (biotinylated HABP, b-HABP, Merck). The samples were subsequently labeled with streptavidin-APC (Abcam) for specific fluorescent detection. Samples were analyzed using a FACS Canto II cytometer (BD Biosciences). Data were evaluated with FlowJo 5 software (BD Biosciences), and the percentage of HA-positive cells and the mean fluorescence intensity (MFI) of HA production were calculated.

5.14 | Determination of HA Accumulation and CD44 Expression in Tumor Spheroids by Fluorescence Microscopy

To quantify HA levels while preserving spheroid structure, fluorescence microscopy was performed [78]. On day 8, at least eight spheroids of each condition were washed, blocked, and incubated overnight at 4°C in a humid chamber with b-HABP. Subsequently, they were incubated for 1 h in the dark at RT with streptavidin-APC (Abcam). Blocking of streptavidin and biotin was performed with reagents from the VectorLab kit (Vector Laboratories). CD44 expression was evaluated by immunofluorescence using a primary mouse antihuman CD44 antibody (1:500, Cell Signaling) followed by an Alexa Fluor 488-conjugated anti-mouse secondary antibody (AF488, 1:500, Cell Signaling). To ensure specific binding, non-specific interactions were blocked with 1% BSA in PBS prior to staining. Spheroids were then incubated with 0.3 μg/mL DAPI for 5 min in the dark to identify cell nuclei. As controls for nonspecific signal, autofluorescence was assessed in unstained samples, as well as in samples incubated with streptavidin-APC or anti-mouse AF488 secondary antibody alone. Spheroids were visualized using an Axio Imager.A2 trinocular fluorescence optical microscope (Carl Zeiss), capturing multiple micrographs of each spheroid.

5.15 | Protein Interaction Network Analysis

STRING v12.0 (http://string-db.org/) was used to generate in silico protein interaction networks for the gene products that were analyzed in our experiments. All interactions were predicted with a high confidence threshold and all active predictive methods were allowed. For the enrichment analysis, STRING implements well-known classification systems such as KEGG were used (Kyoto Encyclopedia of Genes and Genomes) [79].

5.16 | Synergy Assays

MDA-MB-231 and MCF-7 spheroids were treated with varying concentrations of EPI and 4-MU for 3 days. Cell viability was assessed using the MTS Reagent (Abcam) as previously described. Synergy was calculated using the SynergyFinder 3.0 web

15216551, 2025, 11, Downloaded from https://iubmb.onlinelibrary.wiley.com/doi/10.1002/iub.70075 by Daiana L. Viale - UNNOBA Uni Nacional del Noroeste de la Provincia de Buenos A. , Wiley Online Library on [10/11/2025]. See the Terms and Conditions (https://onlinelibrary.wiley.com/terms-and-conditions) on Wiley Online Library for rules of use; OA articles are governed by the applicable Creative Commons License

application, employing the Highest Single Agent (HSA) method [80]. This model states that the expected combination effect is the maximum of the single drug responses at corresponding concentrations. This approach specifically evaluates how 4-MU enhances the effect of EPI by comparing its combined effect to the effect observed with the same dose used in the individual EPI treatment. A synergy score of −10 or lower indicates antagonism, −10 to 10 indicates additivity, and a score of 10 or greater suggests synergy.

5.17 | Statistical Analysis

For statistical analysis, 95% confidence intervals (CIs) were calculated based on the arithmetic mean values and variance (standard error of the mean, SEM) of three independent experiments. Prior to statistical testing, normality and homoscedasticity were assessed to select appropriate tests. To evaluate the statistical significance of differences between obtained values, Student's *t*-tests (independent or paired, as appropriate) were used for comparisons between two groups, while analysis of variance (ANOVA) followed by a post hoc test was employed to evaluate differences among more than two experimental groups. The choice of the post hoc test was dependent on the fulfillment of normality and homoscedasticity assumptions. Pearson or Spearman correlation analysis was performed, depending on the normality of the data. Correlation coefficients above 0.8 (or below −0.8) were considered strong correlations. Statistical analyzes were performed using Prism (GraphPad 5), with a p-value <0.05 indicating statistical significance. The detailed summary of all measurements, including mean ± SEM values and the statistical tests applied for each experimental condition, is provided in Table S2 for MDA-MB-231 spheroids and Table S3 for MCF-7 spheroids.

Acknowledgments

We would like to thank Natalia Menite for expert technical assistance in flow cytometry. We especially thank Dr. Ina Sevic for her collaboration in English grammar. We especially thank Dr. Ángela Bárbaro and Dr. Virginia Pasquinelli for kindly providing the anti-CC3 antibody.

Conflicts of Interest

The authors declare no conflicts of interest.

References

1. C. Belli, D. Trapani, G. Viale, et al., "Targeting the Microenvironment in Solid Tumors," *Cancer Treatment Reviews* 65 (2018): 22–32, https://doi.org/10.1016/j.ctrv.2018.02.004.

2. M. W. Pickup, J. K. Mouw, and V. M. Weaver, "The Extracellular Matrix Modulates the Hallmarks of Cancer," *EMBO Reports* 15 (2014): 1243–1253, https://doi.org/10.15252/embr.201439246.

3. F. M. Spinelli, D. L. Vitale, I. Sevic, and L. Alaniz, "Hyaluronan in the Tumor Microenvironment," *Tumor Microenvironment: Extracellular Matrix Components–Part A* 1245 (2020): 67.

4. M. I. Tammi, S. Oikari, S. Pasonen-Seppänen, K. Rilla, P. Auvinen, and R. H. Tammi, "Activated Hyaluronan Metabolism in the Tumor Matrix – Causes and Consequences," *Matrix Biology* 78 (2019): 147–164, https://doi.org/10.1016/j.matbio.2018.04.012.

5. S. Pushpakom, F. Iorio, P. A. Eyers, et al., "Drug Repurposing: Progress, Challenges and Recommendations," *Nature Reviews. Drug Discovery* 18 (2019): 41–58, https://doi.org/10.1038/nrd.2018.168.

6. S. M. Corsello, J. A. Bittker, Z. Liu, et al., "The Drug Repurposing Hub: A Next-Generation Drug Library and Information Resource," *Nature Medicine* 23 (2017): 405–408.

7. L. Sleire, H. E. Førde-Tislevoll, I. A. Netland, L. Leiss, B. S. Skeie, and P. Ø. Enger, "Drug Repurposing in Cancer," *Pharmacological Research* 124 (2017): 74.

8. A. J. Coukell and D. Faulds, "Epirubicin. An Updated Review of Its Pharmacodynamic and Pharmacokinetic Properties and Therapeutic Efficacy in the Management of Breast Cancer," *Drugs* 53 (1997): 453–482, https://doi.org/10.2165/00003495-199753030-00008.

9. M. Khasraw, R. Bell, and C. Dang, "Epirubicin: Is It Like Doxorubicin in Breast Cancer? A Clinical Review," *Breast* 21 (2012): 142–149.

10. W. L. Sun, J. Chen, Y. P. Wang, and H. Zheng, "Autophagy Protects Breast Cancer Cells From Epirubicin-Induced Apoptosis and Facilitates Epirubicin-Resistance Development," *Autophagy* 7 (2011): 1035–1044, https://doi.org/10.4161/auto.7.9.16521.

11. P. M. Diiffy, M. C. Hayes, A. Cooper, and C. J. Smart, "Determination and Reversal of Resistance to Epirubicin Intravesical Chemotherapy. A Flow Cytometric Model," *British Journal of Urology* 77 (1996): 819–823, https://doi.org/10.1046/j.1464-410x.1996.09038.x.

12. D. G. Hu, A. Rogers, and P. I. Mackenzie, "Epirubicin Upregulates UDP Glucuronosyltransferase 2B7 Expression in Liver Cancer Cells via the P53 Pathway," *Molecular Pharmacology* 85 (2014): 887–897, https://doi.org/10.1124/mol.114.091603.

13. D. Vigetti, M. Ori, M. Viola, et al., "Molecular Cloning and Characterization of UDP-Glucose Dehydrogenase From the Amphibian *Xenopus laevis* and Its Involvement in Hyaluronan Synthesis," *Journal of Biological Chemistry* 281 (2006): 8254–8263, https://doi.org/10.1074/jbc.M508516200.

14. A. Kultti, S. Pasonen-Seppänen, M. Jauhiainen, et al., "4-Methylumbelliferone Inhibits Hyaluronan Synthesis by Depletion of Cellular UDP-Glucuronic Acid and Downregulation of Hyaluronan Synthase 2 and 3," *Experimental Cell Research* 315 (2009): 1914–1923, https://doi.org/10.1016/j.yexcr.2009.03.002.

15. I. Kakizaki, K. Kojima, K. Takagaki, et al., "A Novel Mechanism for the Inhibition of Hyaluronan Biosynthesis by 4-Methylumbelliferone," *Journal of Biological Chemistry* 279 (2004): 33281–33289, https://doi.org/10.1074/jbc.M405918200.

16. D. L. Vitale, A. Icardi, P. Rosales, F. M. Spinelli, I. Sevic, and L. D. Alaniz, "Targeting the Tumor Extracellular Matrix by the Natural Molecule 4-Methylumbelliferone: A Complementary and Alternative Cancer Therapeutic Strategy," *Frontiers in Oncology* 11 (2021): 710061, https://doi.org/10.3389/fonc.2021.710061.

17. B. H. Choi, I. Ryoo, K. H. Sim, H. J. Ahn, Y. J. Lee, and M. K. Kwak, "High Levels of Hyaluronic Acid Synthase-2 Mediate NRF2-Driven Chemoresistance in Breast Cancer Cells," *Biomolecules & Therapeutics* 30 (2022): 368–379, https://doi.org/10.4062/biomolther.2022.074.

18. X. Dai, H. Cheng, Z. Bai, and J. Li, "Breast Cancer Cell Line Classification and Its Relevance With Breast Tumor Subtyping," *Journal of Cancer* 8 (2017): 3131–3141.

19. G. Chen, W. Liu, and B. Yan, "Breast Cancer MCF-7 Cell Spheroid Culture for Drug Discovery and Development," *Journal of Cancer Therapy* 13 (2022): 117–130, https://doi.org/10.4236/jct.2022.133009.

20. Z. Huang, P. Yu, and J. Tang, "Characterization of Triple-Negative Breast Cancer MDA-MB-231 Cell Spheroid Model," *Oncotargets and Therapy* 13 (2020): 5395–5405, https://doi.org/10.2147/OTT.S249756.

21. S. Yoshihara, A. Kon, D. Kudo, et al., "A Hyaluronan Synthase Suppressor, 4-Methylumbelliferone, Inhibits Liver Metastasis of Melanoma

15216551, 2025, 11, Downloaded from https://iubmb.onlinelibrary.wiley.com/doi/10.1002/iub.70075 by Daiana L. Vitale - UNNOBA Uni Nacional del Noroeste de la Provincia de Buenos A , Wiley Online Library on [10/11/2025]. See the Terms and Conditions (https://onlinelibrary.wiley.com/terms-and-conditions) on Wiley Online Library for rules of use; OA articles are governed by the applicable Creative Commons License

Cells," *FEBS Letters* 579 (2005): 2722–2726, https://doi.org/10.1016/j.febslet.2005.03.079.

22. Y. Fang, Y. He, H. Wang, et al., "Hematopoiesis Toxicity Induced by 4-Methylumbelliferon Determined in an Invertebrate Model Organism," *Drug and Chemical Toxicology* 39 (2016): 199–205, https://doi.org/10.3109/01480545.2015.1079915.

23. X. F. Wang, Z. F. Zhao, M. H. Chen, Q. H. Yuan, Y. L. Li, and C. L. Jiang, "Epirubicin Inhibits Growth and Alters the Malignant Phenotype of the U.87 Glioma Cell Line," *Molecular Medicine Reports* 12 (2015): 5917–5923, https://doi.org/10.3892/mmr.2015.4220.

24. E.-M. S. Othman, "Cytogenetic Effect of the Anticancer Drug Epirubicin on Chinese Hamster Cell Line In Vitro," *Mutation Research/Genetic Toxicology and Environmental Mutagenesis* 468 (2000): 109–115, https://doi.org/10.1016/S1383-5718(00)00047-4.

25. G. An, S. Park, M. Lee, W. Lim, and G. Song, "Antiproliferative Effect of 4-Methylumbelliferone in Epithelial Ovarian Cancer Cells Is Mediated by Disruption of Intracellular Homeostasis and Regulation of PI3K/AKT and Mapk Signaling," *Pharmaceutics* 12 (2020): 1–14, https://doi.org/10.3390/pharmaceutics12070640.

26. S. Toldo, R. W. Goehe, M. Lotrionte, et al., "Comparative Cardiac Toxicity of Anthracyclines In Vitro and In Vivo in the Mouse," *PLoS One* 8 (2013): e58421, https://doi.org/10.1371/journal.pone.0058421.

27. F. Piccioni, M. Malvicini, M. G. Garcia, et al., "Antitumor Effects of Hyaluronic Acid Inhibitor 4-Methylumbelliferone in an Orthotopic Hepatocellular Carcinoma Model in Mice," *Glycobiology* 22 (2012): 400–410, https://doi.org/10.1093/glycob/cwr158.

28. J. A. García-Vilas, A. R. Quesada, and M. Á. Medina, "4-Methylumbelliferone Inhibits Angiogenesis In Vitro and In Vivo," *Journal of Agricultural and Food Chemistry* 61 (2013): 4063–4071, https://doi.org/10.1021/jf303062h.

29. R. Saga, Y. Matsuya, R. Takahashi, K. Hasegawa, H. Date, and Y. Hosokawa, "4-Methylumbelliferone Administration Enhances Radiosensitivity of Human Fibrosarcoma by Intercellular Communication," *Scientific Reports* 11 (2021): 8258, https://doi.org/10.1038/s41598-021-87850-3.

30. J. I. Rosser, N. Nagy, R. Goel, et al., "Oral Hymecromone Decreases Hyaluronan in Human Study Participants," *Journal of Clinical Investigation* 132, no. 9 (2022): e157983, https://doi.org/10.1172/JCI157983.

31. N. Nagy, H. F. Kuipers, A. R. Frymoyer, et al., "4-Methylumbelliferone Treatment and Hyaluronan Inhibition as a Therapeutic Strategy in Inflammation, Autoimmunity, and Cancer," *Frontiers in Immunology* 6 (2015): 1–11, https://doi.org/10.3389/fimmu.2015.00123.

32. K. Czepiel, N. Nagy, T. Panjalingam, et al., "Randomised, Placebo-Controlled Trial of Oral Hymecromone in Adults With Pulmonary Hypertension," *Thorax* 80 (2025): 632–640, https://doi.org/10.1136/thorax-2024-222725.

33. N. Nagy, T. Freudenberger, A. Melchior-Becker, et al., "Inhibition of Hyaluronan Synthesis Accelerates Murine Atherosclerosis: Novel Insights Into the Role of Hyaluronan Synthesis," *Circulation* 122 (2010): 2313–2322, https://doi.org/10.1161/CIRCULATIONAHA.110.972653.

34. M. J. Zaya, R. N. Hines, and J. C. Stevens, "Epirubicin Glucuronidation and UGT2B7 Developmental Expression," *Drug Metabolism and Disposition* 34 (2006): 2097–2101, https://doi.org/10.1124/dmd.106.011387.

35. F. Innocenti, L. Iyer, J. Ramírez, M. D. Green, and M. J. Ratain, "Epirubicin Glucuronidation Is Catalyzed by Human UDP-Glucuronosyltransferase 2B7," *Drug Metabolism and Disposition* 29 (2001): 686–692.

36. C. T. Mierke, "Extracellular Matrix Cues Regulate Mechanosensing and Mechanotransduction of Cancer Cells," *Cells* 13 (2024): 96.

37. A. Elosegui-Artola, "The Extracellular Matrix Viscoelasticity as a Regulator of Cell and Tissue Dynamics," *Current Opinion in Cell Biology* 72 (2021): 10–18.

38. S. Ghatak, S. Misra, and B. P. Toole, "Hyaluronan Oligosaccharides Inhibit Anchorage-Independent Growth of Tumor Cells by Suppressing the Phosphoinositide 3-Kinase/Akt Cell Survival Pathway," *Journal of Biological Chemistry* 277 (2002): 38013–38020, https://doi.org/10.1074/jbc.M202404200.

39. T. J. Yates, L. E. Lopez, S. D. Lokeshwar, et al., "Dietary Supplement 4-Methylumbelliferone: An Effective Chemopreventive and Therapeutic Agent for Prostate Cancer," *Journal of the National Cancer Institute* 107 (2015): 1–10, https://doi.org/10.1093/jnci/djv085.

40. N. A. Lokman, Z. K. Price, E. K. Hawkins, A. M. Macpherson, M. K. Oehler, and C. Ricciardelli, "4-Methylumbelliferone Inhibits Cancer Stem Cell Activation and Overcomes Chemoresistance in Ovarian Cancer," *Cancers (Basel)* 11 (2019): 1187, https://doi.org/10.3390/cancers11081187.

41. P. P. Provenzano and S. R. Hingorani, "Hyaluronan, Fluid Pressure, and Stromal Resistance in Pancreas Cancer," *British Journal of Cancer* 108 (2013): 1–8.

42. M. Bakker, W. T. A. van der Graaf, H. J. M. Groen, E. F. Smit, and E. G. E. De Vries, "Anthracyclines – Pharmacology and Resistance, A Review," *Current Pharmaceutical Design* 1 (2022): 133–144, https://doi.org/10.2174/1381612801666220524194324.

43. G. Sgaragli, "ATP-Binding Cassette (ABC) Transporters Are Still Important Drug Targets for Combating Multidrug-Resistant Cancer Cells," *Anticancer Research* 34 (2014): 6160–6162.

44. M. Dean, "ABC Transporters, Drug Resistance, and Cancer Stem Cells," *Journal of Mammary Gland Biology and Neoplasia* 14 (2009): 3–9, https://doi.org/10.1007/s10911-009-9109-9.

45. M. M. Gottesman and I. H. Pastan, "The Role of Multidrug Resistance Efflux Pumps in Cancer: Revisiting a JNCI Publication Exploring Expression of the MDR1 (P-Glycoprotein) Gene," *Journal of the National Cancer Institute* 107 (2015): djv222.

46. S. Misra, S. Ghatak, and B. P. Toole, "Regulation of MDR1 Expression and Drug Resistance by a Positive Feedback Loop Involving Hyaluronan, Phosphoinositide 3-Kinase, and ErbB2," *Journal of Biological Chemistry* 280 (2005): 20310–20315, https://doi.org/10.1074/jbc.M500737200.

47. R. Ohashi, F. Takahashi, R. Cui, et al., "Interaction Between CD44 and Hyaluronate Induces Chemoresistance in Non-Small Cell Lung Cancer Cell," *Cancer Letters* 252 (2007): 225–234, https://doi.org/10.1016/j.canlet.2006.12.025.

48. A. G. Gilg, S. L. Tye, L. B. Tolliver, et al., "Targeting Hyaluronan Interactions in Malignant Gliomas and Their Drug-Resistant Multipotent Progenitors," *Clinical Cancer Research* 14 (2008): 1804–1813, https://doi.org/10.1158/1078-0432.CCR-07-1228.

49. C. Ricciardelli, M. P. Ween, N. A. Lokman, I. A. Tan, C. E. Pyragius, and M. K. Oehler, "Chemotherapy-Induced Hyaluronan Production: A Novel Chemoresistance Mechanism in Ovarian Cancer," *BMC Cancer* 13 (2013): 476, https://doi.org/10.1186/1471-2407-13-476.

50. R. I. Cordo-Russo, L. D. Alaniz, N. Saccodossi, et al., "Hyaluronan Induces Migration of Multidrug-Resistant Lymphoma Cell Lines In Vitro Through Tiam1 Activation by a PI3K-Dependent Mechanism," *Leukemia Research* 34 (2010): 1525–1532, https://doi.org/10.1016/j.leukres.2010.02.020.

51. D. L. Vitale, A. Parnigoni, M. Viola, et al., "Deciphering Drug Resistance: Investigating the Emerging Role of Hyaluronan Metabolism and Signaling and Tumor Extracellular Matrix in Cancer Chemotherapy," *International Journal of Molecular Sciences* 25 (2024): 7607, https://doi.org/10.3390/ijms25147607.

52. A. S. Nunes, A. S. Barros, E. C. Costa, A. F. Moreira, and I. J. Correia, "3D Tumor Spheroids as In Vitro Models to Mimic In Vivo Human Solid

15216551, 2025, 11, Downloaded from https://iubmb.onlinelibrary.wiley.com/doi/10.1002/iub.70075 by Daiana L. Vitale - UNNOBA Uni Nacional del Noroeste de la Provincia de Buenos A , Wiley Online Library on [10/11/2025]. See the Terms and Conditions (https://onlinelibrary.wiley.com/terms-and-conditions) on Wiley Online Library for rules of use; OA articles are governed by the applicable Creative Commons License

Tumors Resistance to Therapeutic Drugs," *Biotechnology and Bioengineering* 116 (2019): 206–226.

53. C. C. Dufort, K. E. DelGiorno, M. A. Carlson, et al., "Interstitial Pressure in Pancreatic Ductal Adenocarcinoma Is Dominated by a Gel-Fluid Phase," *Biophysical Journal* 110 (2016): 2106–2119, https://doi.org/10.1016/j.bpj.2016.03.040.

54. P. Heldin, C. Y. Lin, C. Kolliopoulos, Y. H. Chen, and S. S. Skandalis, "Regulation of Hyaluronan Biosynthesis and Clinical Impact of Excessive Hyaluronan Production," *Matrix Biology* 78–79 (2019): 100–117.

55. T. T. Karalis, P. Heldin, D. H. Vynios, et al., "Tumor-Suppressive Functions of 4-MU on Breast Cancer Cells of Different ER Status: Regulation of Hyaluronan/HAS2/CD44 and Specific Matrix Effectors," *Matrix Biology* 78 (2019): 118–138, https://doi.org/10.1016/j.matbio.2018.04.007.

56. D. Hagiuda, R. Nagashio, M. Ichinoe, et al., "Clinicopathological and Prognostic Significance of Nuclear UGDH Localizatioin Lung Adenocarcinoma," *Biomedical Research (Tokyo)* 40 (2019): 17.

57. B. S. Harrington, R. Kamdar, F. Ning, et al., "UGDH Promotes Tumor-Initiating Cells and a Fibroinflammatory Tumor Microenvironment in Ovarian Cancer," *Journal of Experimental & Clinical Cancer Research* 42 (2023): 270, https://doi.org/10.1186/s13046-023-02820-z.

58. M. J. Price, A. D. Nguyen, J. K. Byemerwa, J. Flowers, C. D. Baëta, and C. R. Goodwin, "UDP-Glucose Dehydrogenase (UGDH) in Clinical Oncology and Cancer Biology," *Oncotarget* 14 (2023): 843–857.

59. C. O. McAtee, J. J. Barycki, and M. A. Simpson, "Emerging Roles for Hyaluronidase in Cancer Metastasis and Therapy," *Advances in Cancer Research* 123 (2014): 1–34.

60. J. T. Posey, M. S. Soloway, S. Ekici, et al., "Evaluation of the Prognostic Potential of Hyaluronic Acid and Hyaluronidase (HYAL1) for Prostate Cancer," *Cancer Research* 63 (2003): 2638–2644.

61. R. Stern, "Hyaluronidases in Cancer Biology," *Seminars in Cancer Biology* 18 (2008): 275–280.

62. V. B. Lokeshwar, D. Rubinowicz, G. L. Schroeder, et al., "Stromal and Epithelial Expression of Tumor Markers Hyaluronic Acid and HYAL1 Hyaluronidase in Prostate Cancer," *Journal of Biological Chemistry* 276 (2001): 11922–11932, https://doi.org/10.1074/jbc.M008432200.

63. H. Bouga, I. Tsouros, D. Bounias, et al., "Involvement of Hyaluronidases in Colorectal Cancer," *BMC Cancer* 10 (2010): 499, https://doi.org/10.1186/1471-2407-10-499.

64. Y. Yan, X. Zuo, and D. Wei, "Concise Review: Emerging Role of CD44 in Cancer Stem Cells: A Promising Biomarker and Therapeutic Target," *Stem Cells Translational Medicine* 4 (2015): 1033–1043, https://doi.org/10.5966/sctm.2015-0048.

65. D. Park, Y. Kim, H. Kim, et al., "Hyaluronic Acid Promotes Angiogenesis by Inducing RHAMM-TGFβ Receptor Interaction via CD44-PKCδ," *Molecular Cell* 33 (2012): 563–574, https://doi.org/10.1007/s10059-012-2294-1.

66. N. Nagy, I. Gurevich, H. F. Kuipers, et al., "4-Methylumbelliferyl Glucuronide Contributes to Hyaluronan Synthesis Inhibition," *Journal of Biological Chemistry* 294 (2019): 7864–7877, https://doi.org/10.1074/jbc.RA118.006166.

67. T. Liu, L. Zhou, D. Li, T. Andl, and Y. Zhang, "Cancer-Associated Fibroblasts Build and Secure the Tumor Microenvironment," *Frontiers in Cell and Developmental Biology* 7 (2019): 60.

68. R. Kalluri, "The Biology and Function of Fibroblasts in Cancer," *Nature Reviews. Cancer* 16 (2016): 582–598.

69. K. C. Valkenburg, A. E. De Groot, and K. J. Pienta, "Targeting the Tumour Stroma to Improve Cancer Therapy," *Nature Reviews. Clinical Oncology* 15 (2018): 366–381.

70. W. Knudson, C. Biswas, and B. P. Toole, "Interactions Between Human Tumor Cells and Fibroblasts Stimulate Hyaluronate Synthesis," *Proceedings of the National Academy of Sciences of the United States of America* 81 (1984): 6767–6771, https://doi.org/10.1073/pnas.81.21.6767.

71. Z. Liu, P. Hou, J. Fang, et al., "Mesenchymal Stromal Cells Confer Breast Cancer Doxorubicin Resistance by Producing Hyaluronan," *Oncogene* 42 (2023): 3221–3235, https://doi.org/10.1038/s41388-023-02837-w.

72. L. Yin, J. J. Duan, X. W. Bian, and S. C. Yu, "Triple-Negative Breast Cancer Molecular Subtyping and Treatment Progress," *Breast Cancer Research* 22 (2020): 61.

73. W. Yue and A. Brodie, "MCF-7 Human Breast Carcinomas in Nude Mice as a Model for Evaluating Aromatase Inhibitors," *Journal of Steroid Biochemistry and Molecular Biology* 44 (1993): 671–673, https://doi.org/10.1016/0960-0760(93)90278-5.

74. A. d. L. Mota, A. F. Evangelista, T. Macedo, et al., "Molecular Characterization of Breast Cancer Cell Lines by Clinical Immunohistochemical Markers," *Oncology Letters* 13 (2017): 4708–4712, https://doi.org/10.3892/ol.2017.6093.

75. D. L. Vitale, F. M. Spinelli, D. Del Dago, et al., "Co-Treatment of Tumor Cells With Hyaluronan Plus Doxorubicin Affects Endothelial Cell Behavior Independently of VEGF Expression," *Oncotarget* 9 (2018): 36585–36602, https://doi.org/10.18632/oncotarget.26379.

76. E. C. Costa, A. F. Moreira, D. de Melo-Diogo, V. M. Gaspar, M. P. Carvalho, and I. J. Correia, "3D Tumor Spheroids: An Overview on the Tools and Techniques Used for Their Analysis," *Biotechnology Advances* 34 (2016): 1427–1441.

77. D. L. Vitale, F. M. Spinelli, and L. Alaniz, "Determination of Cell-Surface Hyaluronan Through Flow Cytometry," *Methods in Molecular Biology* 1952 (2019): 111–116.

78. F. M. Spinelli, P. Rosales, S. Pluda, et al., "The Effects of Sulfated Hyaluronan in Breast, Lung and Colorectal Carcinoma and Monocytes/Macrophages Cells: Its Role in Angiogenesis and Tumor Progression," *IUBMB Life* 74, no. 10 (2022): 927–942, https://doi.org/10.1002/iub.2604.

79. D. Szklarczyk, A. L. Gable, D. Lyon, et al., "STRING V11: Protein-Protein Association Networks With Increased Coverage, Supporting Functional Discovery in Genome-Wide Experimental Datasets," *Nucleic Acids Research* 47 (2019): D607–D613, https://doi.org/10.1093/nar/gky1131.

80. A. Ianevski, A. K. Giri, and T. Aittokallio, "SynergyFinder 3.0: An Interactive Analysis and Consensus Interpretation of Multi-Drug Synergies Across Multiple Samples," *Nucleic Acids Research* 50 (2022): W739–W743, https://doi.org/10.1093/nar/gkac382.

Supporting Information

Additional supporting information can be found online in the Supporting Information section. **Figure S1:** Representative bright-field images of MDA-MB-231 spheroids after dissociation and re-plating on gelatin-coated supports. (A) Single-cell suspensions obtained through gentle mechanical dissociation. (B) Re-plated spheroids after 48 h of culture, illustrating cell adhesion and spreading. **Figure S2:** Representative bright-field images of MCF-7 spheroids after dissociation and re-plating on gelatin-coated supports. (A) Single-cell suspensions obtained through gentle mechanical dissociation. (B) Re-plated spheroids after 48 h of culture, illustrating cell adhesion and spreading. **Figure S3:** Summary of the flow cytometry (FACS) gating strategy applied to all experiments. Sequential gating steps were used to exclude debris, doublets, and dead cells, allowing analysis of a homogeneous population of single viable cells. **Figure S4:** Activation of caspase-3 in response to 4-MU and EPI treatment in MDA-MB-231 spheroids. MDA-MB-231 cells (8×10^3) were cultured under three-dimensional conditions using the hanging drop assay to allow the formation of tumor spheroids. On day 5, the spheroids were treated with 0.5 mM 4-MU plus 2.5 μM EPI for 3 days. On day 8, different spheroids per condition were collected and cleaved caspase-3 (CC3) expression was determined by intracytoplasmic flow cytometry. Bars show the percentage of CC3+ cells (B) or the

15216551, 2025, 11, Downloaded from https://iubmb.onlinelibrary.wiley.com/doi/10.1002/iub.70075 by Daiana L. Vitale - UNNOBA Uni Nacional del Noroeste de la Provincia de Buenos A. Wiley Online Library on [10/11/2025]. See the Terms and Conditions (https://onlinelibrary.wiley.com/terms-and-conditions) on Wiley Online Library for rules of use; OA articles are governed by the applicable Creative Commons License

mean fluorescence intensity (MFI) (C) determined by comparison with a negative control. Histograms (A) show the most representative experiment performed with at least 50,000 events/condition. $N = 4$, expressed as mean ± SEM. *$p < 0.05$, **$p < 0.01$. **Figure S5:** Analysis of EPI accumulation and HA pericellular accumulation by flow cytometry. MDA-MB-231 or MCF-7 cells (8×10^3) were cultured under three-dimensional conditions using the hanging drop assay to allow the formation of tumor spheroids. On day 5, spheroids were treated with 0.5 mM 4-MU plus 2.5 μM EPI for 3 days. On day 8, different spheroids per condition were harvested and HA pericellular accumulation and EPI accumulation were determined by flow cytometry. Dot plots show the most representative data. Scale bar: 200 μm. Mean ± SEM. *$p < 0.05$, **$p < 0.01$, ***$p < 0.001$, ****$p < 0.0001$. **Table S1:** Primers used for RT-qPCR. **Table S2:** Summary of statistical analyzes for MDA-MB-231 spheroids, including mean ± SEM and the statistical tests applied for each experimental condition. **Table S3:** Summary of statistical analyzes for MCF-7 spheroids, including mean ± SEM and the statistical tests applied for each experimental condition.

15216551, 2025, 11, Downloaded from https://iubmb.onlinelibrary.wiley.com/doi/10.1002/iub.70075 by Daiana L. Viale - UNNOBA Uni Nacional del Noroeste de la Provincia de Buenos A , Wiley Online Library on [10/11/2025]. See the Terms and Conditions (https://onlinelibrary.wiley.com/terms-and-conditions) on Wiley Online Library for rules of use; OA articles are governed by the applicable Creative Commons License